3-D Restoration of Complexly Folded and Faulted Surfaces Using Multiple Unfolding Mechanisms[1]

Delphine Rouby,[2] Hongbin Xiao,[3] and John Suppe[4]

ABSTRACT

The ability to extract the history of motions associated with geologic structures is a key element in understanding fundamental deformation processes, for example, the growth of folds or faults in three dimensions, the interactions between faults, and the spatial relationships between deformation and sedimentation. Here, we show how to extract these motions for complexly faulted and folded structures using a new method of three-dimensional (3-D) restoration.

We perform the restoration on sets of stratigraphic horizons defined in three dimensions as irregular triangular networks (triangulated surfaces), with the unfaulting and unfolding as separate steps. The unfolding is achieved by a best-fit packing of the triangular surface elements, implementing several restoration mechanisms, including (1) flexural slip, (2) homogeneous inclined shear, and (3) 3-D inclined shear oriented in the azimuth of the local surface dip. After unfolding, we restore the displacement on the faults in map view by a best-fit rigid-body packing of fault blocks in a way that allows for complex systems of faults. By performing the combined unfolding and unfaulting with multiple orientations of the unfolding vectors, we determine the optimum combination of unfolding plus unfaulting, which yields a best estimate of the surface-strain fields, the particle-displacement field, and the fault-slip vectors in three dimensions.

We illustrate the restoration method with synthetic examples and a complexly faulted structure from the western Niger Delta that is imaged in 3-D seismic data. We include the results of tests to quantify some potential sources of error in the restorations.

INTRODUCTION

The ability to quantify the motions associated with geologic deformation provides fundamental insight into the growth of folds or faults in three dimensions, the interactions between faults, and the kinematics and spatial relationships between processes of deformation and sedimentation. Displacement fields of tectonically active structures can be determined on a short time scale by geodetic measurement; however, for most geological structures, restoration methods are required. Proper restorations allow the structural geologist to reconstruct the undeformed geometry of well-imaged structures assuming balancing constraints and deformation mechanisms. In doing so, structural geologists can check the consistency of their interpretations, assumed deformation mechanisms, and chosen boundary conditions. The difference between the restored and deformed states gives the finite displacements, strains, rotations, and fault slip, which are fundamental constraints for analyzing the deformation processes and the quantification of the structure kinematics. The measures of the deformation can also be used, especially for oil-industry purposes, to predict areas that have undergone larger strains at the subseismic (reservoir) scale.

Most restoration has been performed in two dimensions, either in cross section or in map view, based on area conservation and additional constraints that are appropriate to specific deformation regimes. Examples include (1) unstraining in map view by heterogeneous shear for ductile deformation regimes (Schwerdtner, 1977; Cobbold and Percevault, 1983), (2) unfolding in cross section by flexural slip (Dahlstrom, 1969; Hossack, 1979) or by vertical or inclined shear (Verral, 1981; Gibbs,

[1]Manuscript received March 23, 1998; revised manuscript received August 2, 1999; final acceptance November 15, 1999.

[2]Princeton 3D Structure Project, Department of Geosciences, Princeton University, Princeton, New Jersey 08544. Present address: Géosciences Rennes, UPR 4661 CNRS, Campus de Beaulieu, 35042 Rennes Cédex, France; e-mail: Delphine.Rouby@univ-rennes1.fr

[3]Chevron CPTC, P.O. Box 6012, San Ramon, California 94583.

[4]Princeton 3D Structure Project, Department of Geosciences, Princeton University, Princeton, New Jersey 08544.

We are grateful to Chevron management for financial support to this study as a part of Strategic Research. We thank Chevron Nigeria Limited for providing us with this data set of a growth fault of the Niger delta. We also thank the Geology Department and the Earth Modeling Team of Chevron Petroleum Technology Company for geological expertise and technical support, especially Eric May, Bill Higgs, Wayne Narr, Jim Phelps, Ken Kelsh, Michele Lo, Steve Garrett, Chuck Sword, Amy Cheng, and Dick Jones. We are grateful to Alan Gibbs, Neil Hurley, John Shaw, Daniel Schultz-Ela, and Richard Stanley for the significant time they spent reviewing the manuscript and for their very helpful suggestions.

1983; White et al., 1986; Schultz-Ela, 1992), and (3) unfaulting in map view by rigid-body translation and rotation of fault blocks (Dokka and Travis, 1990; Audibert, 1991; Richard, 1993; Rouby et al., 1993a, b, 1996a, b; Rouby and Cobbold, 1996; Bourgeois et al., 1997; de Urreiztieta et al., 1996). Restoration in cross section is applicable only to the case of plane bulk strain because the preservation of the area in cross section requires no displacement in or out of the cross section. Methods of restoration in map view, however, can be applied to any type of structures, including domains that do not exhibit plane bulk strains.

Two-dimensional methods of restoration were naturally developed first because of the traditional emphasis on maps and cross sections, which is rooted in the approximately cylindrical nature of many structures, and because of the greater ease of solving two-dimensional (2-D) problems; nevertheless, 3-D data sets have existed for years in the form of dense borehole data and complex mine and surface geologic mapping. Only now have computational power and visualization capabilities reached appropriate levels to contemplate practical and quantitative 3-D restorations; furthermore, new investigative techniques, such as 3-D seismic surveys and digital elevation models, provide structural geologists with an increasing number of comprehensive 3-D data sets in digital format. Integration software brings together these different types of data in a consistent format that is suitable for quantitative structural analysis. Thus, the time is ripe for developing 3-D restoration methods.

Unfolding methods for 3-D surfaces have been recently proposed based on two deformation mechanisms: flexural slip (i.e., surface area conservation) (Gratier et al., 1991; Guillier, 1991; Gratier and Guillier, 1993; Samson, 1996; Williams et al., 1997) and homogeneous inclined shear (shear along vectors with constant inclination and azimuth) (Kerr et al., 1993; Kerr and White, 1996); furthermore, commercial software is available to restore in three dimensions based on the following approximations: (1) solving the restoration problem in 2-D cross sections with interpolation between the sections, (2) limiting the number of faults, and (3) specifying the direction of slip on the faults, which is generally not known.

Here, we present a method of optimized 3-D restoration of both folding and faulting of stratigraphic surfaces based on truly 3-D deformation processes (not the sum of 2-D cross sections), especially when complex fault patterns are involved. The scope of this paper is to describe a new restoration method, and to illustrate its application to some synthetic examples and a natural example based on 3-D seismic imaging of a growth fault system in the western Niger Delta. We implement and compare the different unfolding mechanisms, discuss their validity, and examine the sensitivity of the method to the inclination of the folding vectors and to the boundary conditions.

3-D DEFORMATION PROCESSES

Widespread 3-D seismic surveys now precisely constrain the shapes of many folded and faulted stratigraphic horizons; however, correct restoration of these horizons, and the volumes they enclose, remains a difficult problem. Proper restoration requires the geometrical description of the actual 3-D deformation processes, which are not well understood; nevertheless, the substantial experience that exists in 2-D restoration in map view and cross section provides a good starting point for developing 3-D restoration approach.

Folding Mechanism in Three Dimensions

Two main folding mechanisms are now widely accepted and used in restoration and forward modeling of cross sections: (1) flexural slip for compressional domains and competent rocks where the bed length and thickness are preserved during the deformation and (2) shear along vertical or inclined vectors in extension (Verral, 1981; Gibbs, 1983; White at al., 1986). These 2-D deformation mechanisms have been adapted to the problem of 3-D restoration.

Gratier et al. (1991) unfolded 3-D surfaces by flexural slip using a technique that minimizes the changes in surface area and line length during unfolding. They used a finite element procedure applied to a regular triangular mesh (built from gridded data) that represents the shape of the surface. The triangular elements are rotated individually to horizontal about an axis parallel to strike, then the dispersed triangles are iteratively packed back together while minimizing the voids and overlaps. Williams et al. (1997) modified this approach by minimizing gaps between triangles using the sum of a rigid translation, a rigid rotation, and a constant-area shear strain of each triangle. In an alternative technique, Samson (1996) unfolded surfaces represented by an irregular triangulated mesh (triangulated surfaces) by minimizing the changes in lengths of the sides of the triangles. We include flexural slip based on Gratier et al.'s (1991) implementation as one of our unfolding options.

Kerr et al. (1993) and Kerr and White (1996) assumed that extensional deformation within the hanging wall of a listric fault can be described by a shear along inclined vectors showing constant inclination and azimuth. We include this homogeneous 3-D inclined shear as one of our unfolding

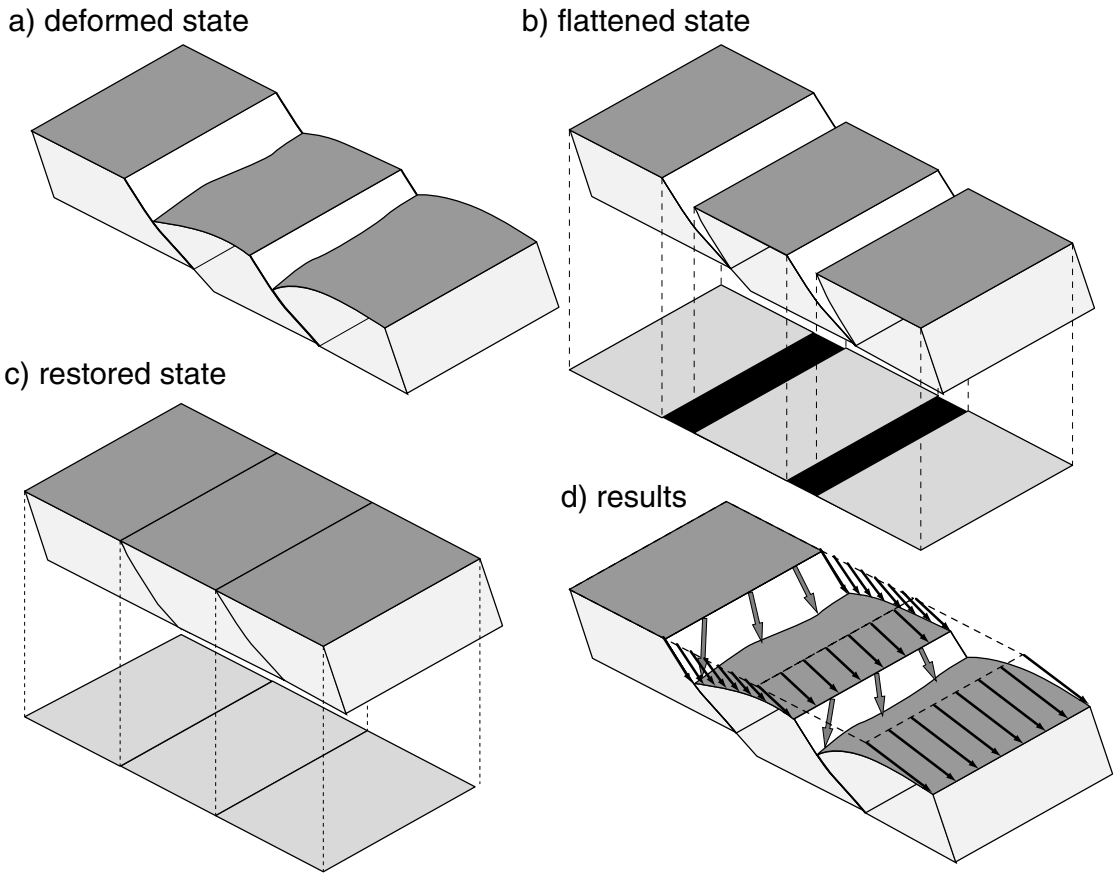

Figure 1—Principle of the restoration method. (a) Initial data are stratigraphic horizons represented by triangulated surfaces (surfaces composed of triangular elements, darker shaded surface) offset by the faults (unshaded surfaces). (b) We first unfold the horizon by choosing among three deformation mechanisms (see text). (c) After unfolding, unfaulting is performed in map view. Before unfaulting, normal faults appear as gaps separating fault compartments (reverse faults appears as overlaps between fault blocks). To invert the displacement on the fault we close the fault gaps by rigid-body motion of the fault compartments. (d) The difference between the deformed and the restored state gives the 3-D finite displacement field (black arrows) and the directions of slip on the faults (shaded arrows).

options. This assumption of homogeneous 3-D inclined shear may be satisfactory for the hanging wall of a single, quasicylindrical listric fault, but it is probably inappropriate for the hanging wall of an irregular fault surface in, for example, faults that include both concave and convex fault bends (see Xiao and Suppe, 1992) or for highly 3-D networks of faults. There is no reason to assume that the folding directions above an irregular fault surface should be homogeneous or that they should be constant from one fault to another within a complex 3-D fault network. Thus, to consider these cases, we include a model of heterogeneous inclined shear (in addition to homogeneous 3-D inclined shear). For the heterogeneous shear, the azimuth of the unfolding vector is parallel to the local dip azimuth of the surface.

Faulting Mechanism in Three Dimensions

The displacement on faults primarily involves rigid-body motion of the fault blocks. If the internal strain of the fault blocks, including tilting and folding, is first removed, then the inversion of the displacement on the faults can be addressed in map view (Figure 1). Indeed, map-view methods of restoration involving rigid motion of fault blocks have been successfully applied in a wide variety of settings, including strike slip (Dokka and Travis, 1990; Audibert, 1991; Richard, 1993), extensional (Rouby et al., 1993a, b, 1996a, b; Rouby and Cobbold, 1996), and compressional (de Urreiztieta, 1996; de Urreiztieta et al., 1996; Bourgeois et al., 1997) environments. Those studies with excellent data demonstrate a high degree of rigid-body fault-block motion (e.g., Rouby

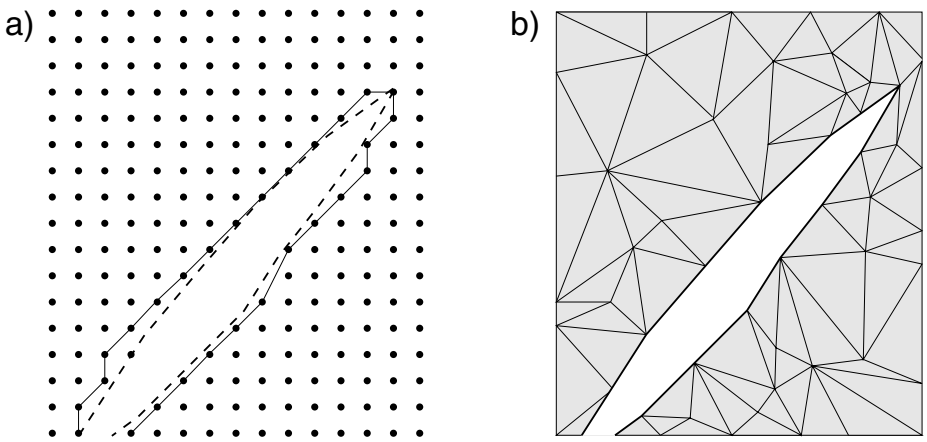

Figure 2—Fault cutoff built on (a) a gridded surface and (b) a triangulated surface. Fault cuts are more precisely defined on a triangulated surface, and the shape of the surface is represented with less information.

et al., 1996a). Thus, we implemented rigid-body motion for the unfaulting step in our 3-D restoration approach.

COMBINED UNFOLDING AND UNFAULTING RESTORATION

Restoration Strategy

To restore folded and complexly faulted 3-D volumes, we apply the following simplifications:

(1) Individual stratigraphic horizons (i.e., surfaces) are restored independently rather than by a full volumetric restoration (Figure 1). Thus, the restoration focuses on the primary data that are used to constrain the shapes of the deformed and faulted horizons, for example, the horizon and fault picks from 3-D seismic data. A shortcoming of this approach is that layer thickness is not used as a constraint in restoration; however, full volumetric restoration is beyond the scope of this paper. We also do not use the shape of the fault surface for various reasons that are stated in the discussion.

(2) We decompose the restoration into two separate steps, unfolding then unfaulting, a method that allows the use of different deformation mechanisms for the two steps. In doing so we base our approach on two existing methods that have been extensively tested, demonstrating their reliability and robustness in case studies.

We perform the unfolding by best-fitting of finite triangular elements following the flexural-slip method of Gratier et al. (1991) previously discussed; however, we increased the flexibility of the method by implementing several unfolding mechanisms so that (1) the method can be applied in different structural environments (either compressional or extensional) and (2) the user can choose the deformation mechanism that provides the best results. We have implemented three different unfolding mechanisms: (1) flexural slip, (2) homogeneous inclined shear, and (3) heterogeneous inclined shear along inclined vectors of constant inclination but variable azimuth controlled by the local dip of the surface.

For the unfaulting step, we restore the fault displacement in map view by fitting of polygonal elements assuming rigid-body motion of fault blocks following Rouby et al. (1993a).

Data

We represent the deformed stratigraphic horizons as irregular triangulated surfaces with gaps corresponding to fault cutoffs (Figure 2b). This format is more flexible than gridded surfaces because the density of control points may vary; it can be higher in areas showing higher curvature and lower in areas showing a more even topography; furthermore, the fault traces are more precisely defined (compare Figure 2a and b).

The accuracy of the fault cutoff is very important for the quality of the restoration because the total displacement field is typically dominated by fault slip. Fault gaps based on seismic mapping can be problematic. Seismic interpreters have to interrupt their horizon picking before reaching the actual fault, stopping at the boundary of the poorly imaged deformed zone (Figure 3a). If we build the horizon surface and the fault gaps directly from these interpreted points, we generally overestimate the horizontal component of dip slip on the faults (Figure 3b). If we build a continuous surface from the interpreted points and then cut the triangulated surface by the fault, we underestimate the horizontal component of dip slip (Figure 3c). To avoid these pitfalls, our procedure is to (1) compute the intersection between the fault and the surface by

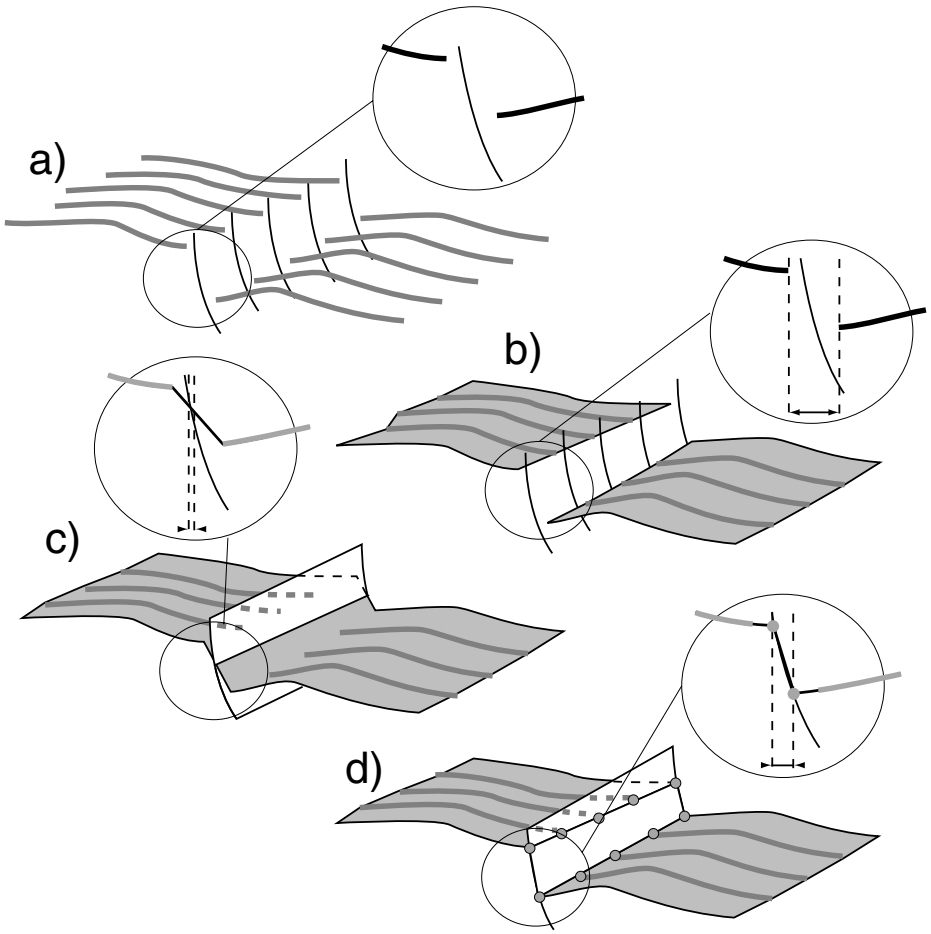

Figure 3—Construction of a triangulated surface offset by faults from interpreted seismic sections. (a) Horizon picking on seismic (darker shaded lines) is usually interrupted before reaching the actual fault. (b) Surface (lighter shaded surface) and fault gaps constructed directly from the interpreted points overestimates the horizontal component of dip-slip on the faults. (c) A continuous surface (lighter shaded surface) constructed from the interpreted points (darker shaded lines) then cut by the fault (unshaded surface) underestimates the horizontal component of slip. (d) The appropriate procedure is to (1) compute the intersection between the fault and the surface by extrapolation (shaded dots), (2) build a continuous surface using both the interpreted points and the intersection points, and (3) cut the triangulated surface by the fault.

extrapolation, (2) build a continuous surface using both the interpreted points and the intersection points, and (3) cut the triangulated surface by the fault. In doing so, we build an accurate fault cutoff (Figure 3d) assuming the fault dip is correct. In our case studies, we have generated the triangulated surfaces and the fault cuts within the GOCAD® 3-D earth modeling software (Mallet, 1992) starting with the horizon and fault picks from 3-D seismic mapping.

Unfolding Step

The first step of the restoration is to unfold the horizon. We flatten each triangle of the triangulated surface separately according to an unfolding mechanism (Figure 4). We have used the following three mechanisms, but others are geologically conceivable: (1) For flexural slip, the area of the surface has to be preserved, so we rotate the triangle about a horizontal axis perpendicular to the dip direction (Gratier et al., 1991). (2) For homogeneous inclined shear, we shear the triangles separately along the same vector defined by the user (both inclination and azimuth). (3) For heterogeneous inclined shear, each triangle is sheared along a vector with an inclination defined by the user and an azimuth defined by the dip azimuth of the triangle.

After the flattening, we obtain a set of triangles showing gaps and overlaps (the "scattered surface" in Figures 4d and 5c). To retrieve the continuity of the surface, we pack the triangles using rigid body rotations and translations designed to reach the least-square minimization of gaps and overlaps (Figure 5d). Triangles are packed sequentially starting from an initial "seed" (stationary point) defining the stationary boundary and a pin line that is flattened first and then remains stationary (Figure 4e). The packing is iterative and monotonically converging, with most of the convergence achieved within the first ten cycles through the entire set of triangles. Excellent packing achieved within 50–100 iterations (Figure 4f).

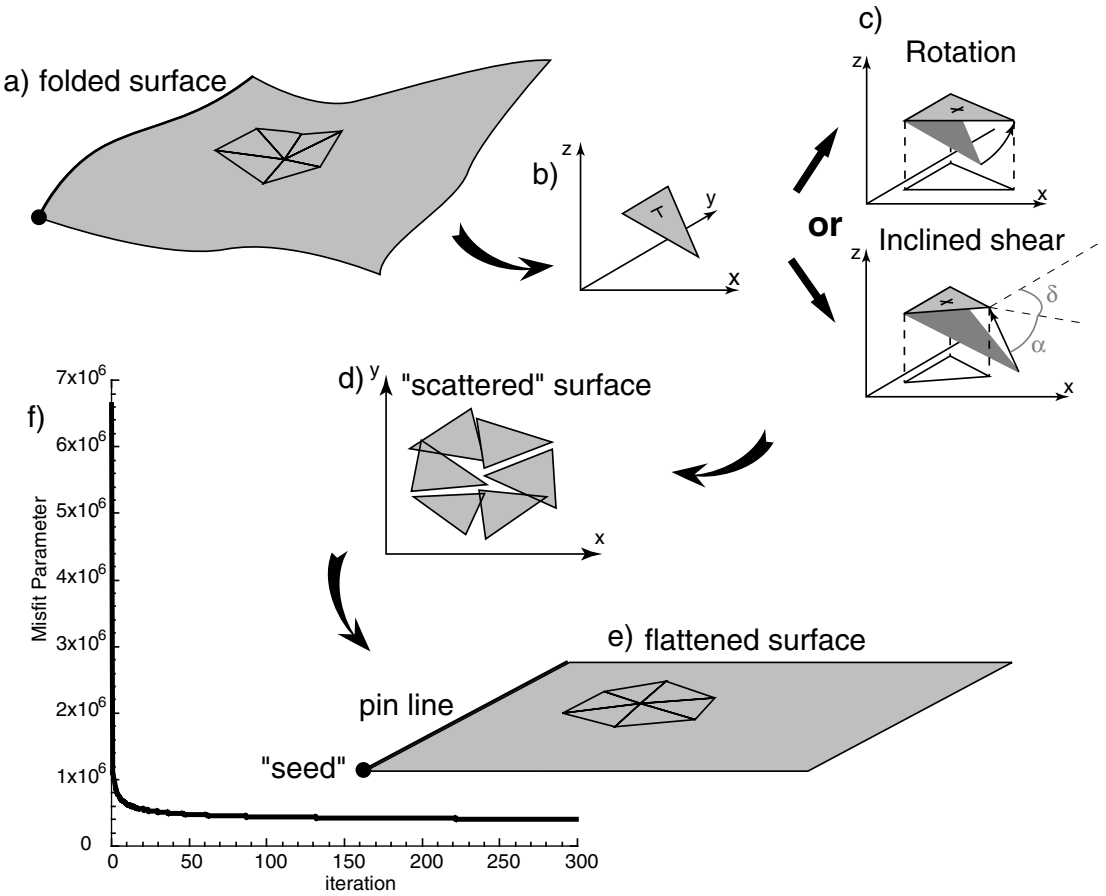

Figure 4—Unfolding of (a) a triangulated surface. Each triangle (b) of the surface is flattened separately. (c) For flexural slip, the triangle is rotated about a horizontal axis perpendicular to the dip direction. For homogeneous inclined shear, the triangle is sheared along a vector defined by the user (both inclination α and azimuth δ). For heterogeneous inclined shear, the triangle is sheared along a vector with an inclination α defined by the user and an azimuth δ defined by the dip azimuth of the triangle. (d) Flattened triangles show gaps and overlaps (the "scattered" surface). (e) Triangles are packed sequentially starting from an initial "seed" and pin line defining the stationary boundary using rigid body rotations and translations (designed to reach the least-square minimization of gaps and overlaps). (f) The iterative packing is monitored by a misfit parameter proportional to the square of the distances between triangle vertices.

After packing the triangles, some gaps and overlaps may remain and necessarily so if the original surface was noncylindrical (nondevelopable), which is to say that it cannot be unfolded without being strained (Figure 5d). We reconstruct a continuous triangulated surface (Figure 5e) by changing slightly the shape and area of the triangles. The vertices of triangles that were located at the same point before unfolding are moved to a common location, which is their centroid. The difference between the initial triangulated surface and this smoothed triangulated surface gives (1) the field of finite displacements corresponding to the unfolding step (the folding vectors) (Figures 6b, 7a, 8c) and (2) the fields of finite strain and dilation corresponding to the change in shape and area of the triangles, which is the surface strain resulting from the unfolding (Figures 5f, g; 7b). If the surface has been unfolded by flexural slip, then this measured strain is related only to the discrepancies of the triangles after the packing procedure (triangles are rotated rigidly to the horizontal); however, when inclined shear is applied, the computed shear strain also involves the component of shear necessary to flatten the triangles.

This strain field can be used to evaluate the quality of the restoration. Areas of high strain can be related to misinterpretation of the horizon surface, to quality problems on the 3-D triangulated surfaces (bad triangulation can lead to artificially high strain values), or to the accuracy of the deformation mechanism

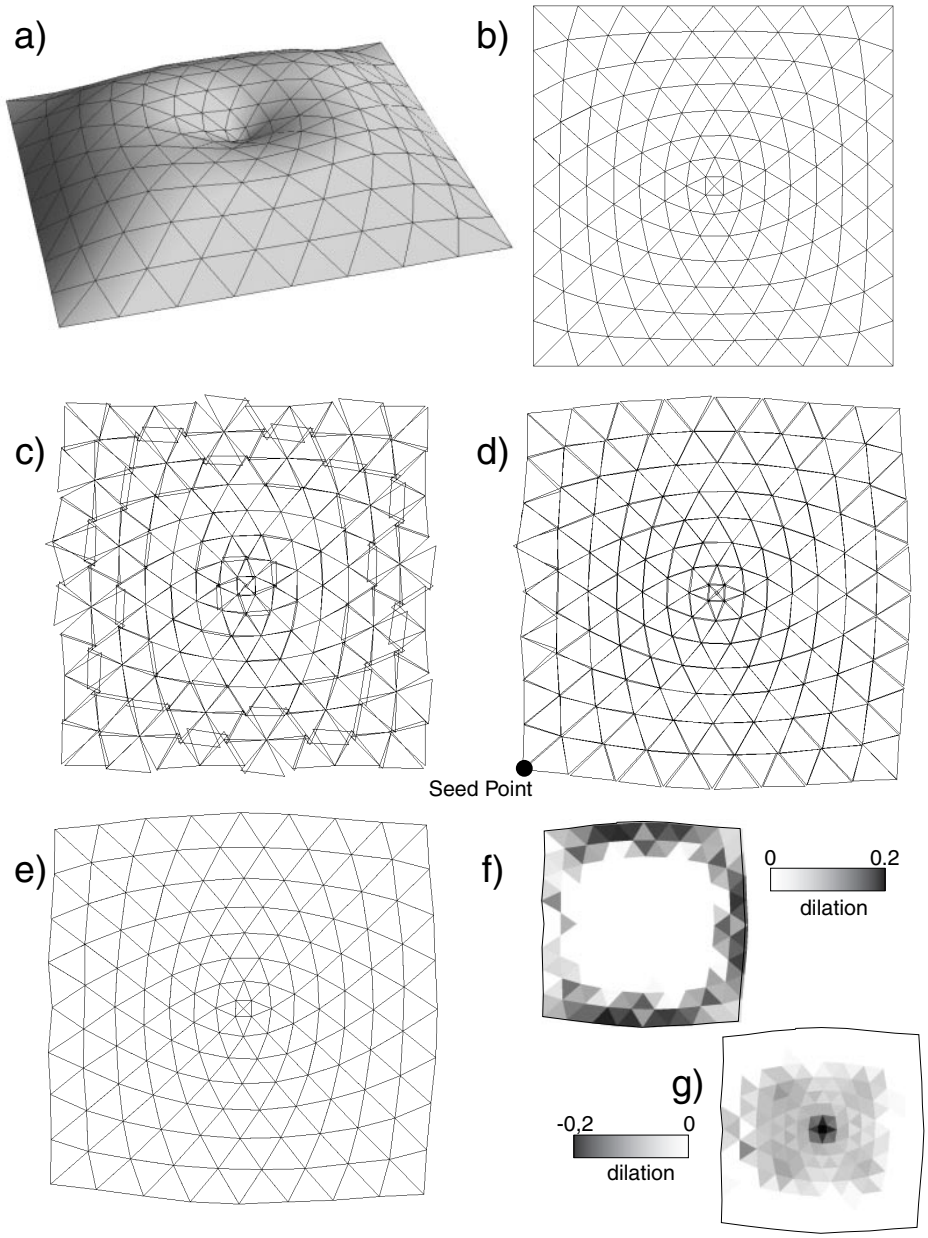

Figure 5—Unfolding of a noncylindrical (nondevelopable) surface by flexural slip. (a) Perspective view of the folded surface. Top view of the surface (b) in the deformed state, (c) after rotation of the triangles to horizontal, and (d) after packing of the triangles. The pin line is located on the left side of the surface with a seed located at the lower left corner (black dot). (e) Top view of the surface after smoothing of the triangles. (f) Map of the positive surface dilation of the triangles between the packed and the smoothed state of surface. (g) Map of the negative surface dilation of the triangles.

chosen; however, once these parameters have been checked and their effects minimized, the strain field can also be used to detect and quantify potential high-strain areas within the structure. These strains occur at scales below the seismic resolution, that is, at the reservoir scale. This prediction can be of significant interest to define reservoir quality and geometry, especially in fractured reservoir, and has bearing on the integrity of hydrocarbon seals.

To illustrate the unfolding procedures, we present a series of figures showing unfolding restoration for various cylindrical and noncylindrical surfaces. Figure 5 illustrates the unfolding by flexural slip of a noncylindrical surface. Note that the perimeter of the surface stretches and dilates upon restoration, whereas the center contracts. Figure 6 illustrates unfolding by flexural slip for a cylindrical surface. Figure 7 illustrates unfolding by homogeneous inclined shear of a cylindrical surface above a normal fault, whereas Figure 8 illustrates unfolding by heterogeneous inclined shear of a noncylindrical surface. Note that the displacement vectors tend to

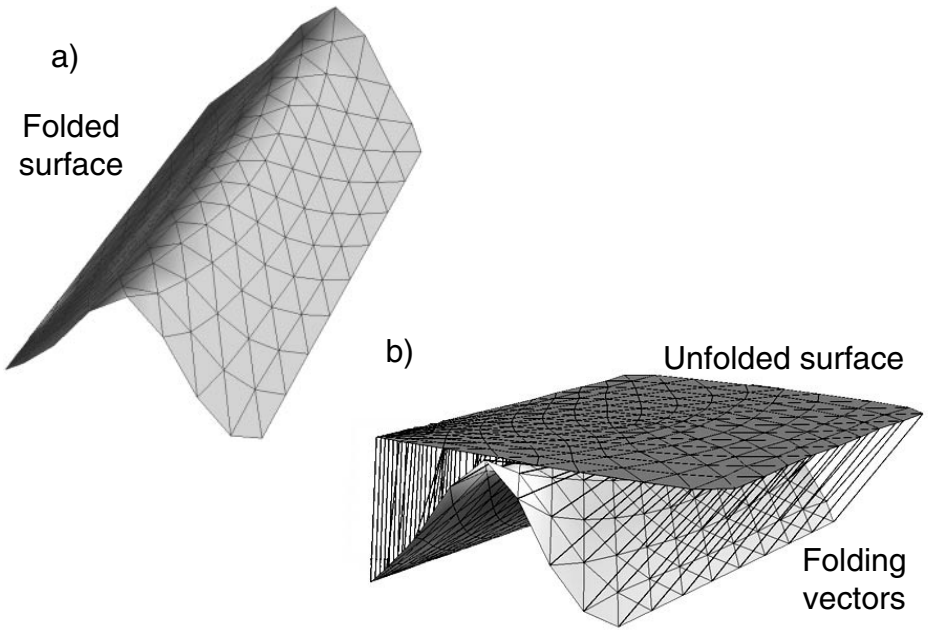

Figure 6—Unfolding of a cylindrical surface (paper sheet) by flexural slip. Perspective view of the (a) folded surface and (b) folded and unfolded surfaces and displacement of the points (folding vectors).

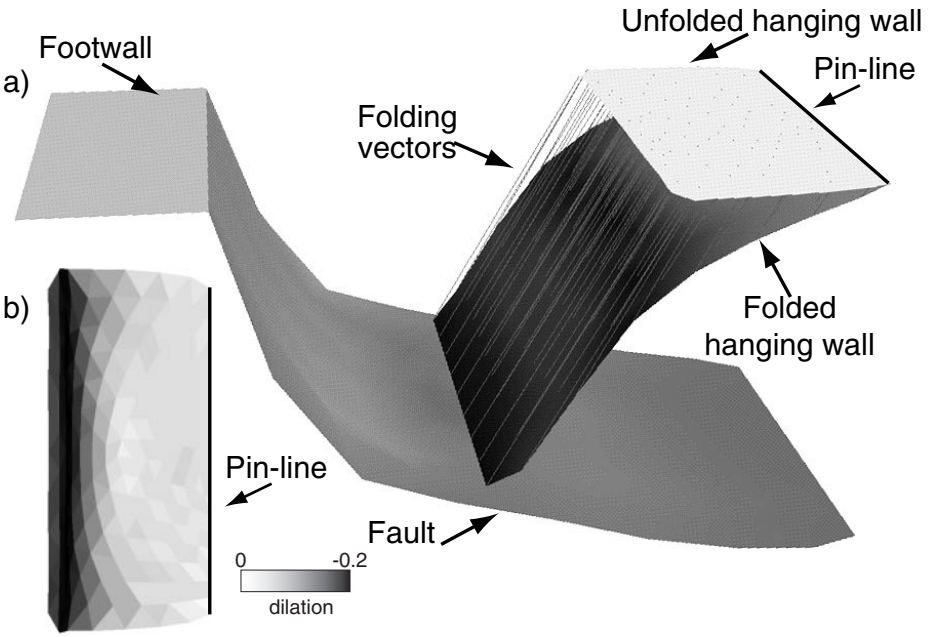

Figure 7—Unfolding of a cylindrical surface by homogeneous inclined shear. (a) Perspective view of the fault, footwall, and folded and unfolded hanging wall. (b) Map of surface dilation associated with the unfolding (negative values). Because of the inclined shear, the areas initially showing larger dip are the areas showing the larger values of negative surface dilation.

be perpendicular to the topographic contour lines in map view (Figure 8c).

Unfaulting Step

After unfolding, we remove the displacement on the faults in map view using the method of Rouby et al. (1993a). This method assumes that the fault displacement is achieved by rigid-body motion of the fault blocks, an assumption that is well justified by the goodness of fit achieved in restoration of excellent data in several case studies (e.g., Rouby et al., 1996a).

From the flattened surface (Figure 9a), we build a mosaic of fault-bounded blocks (Figure 9b) by extrapolating fault traces and adding artificial block boundaries. Normal faults become gaps between

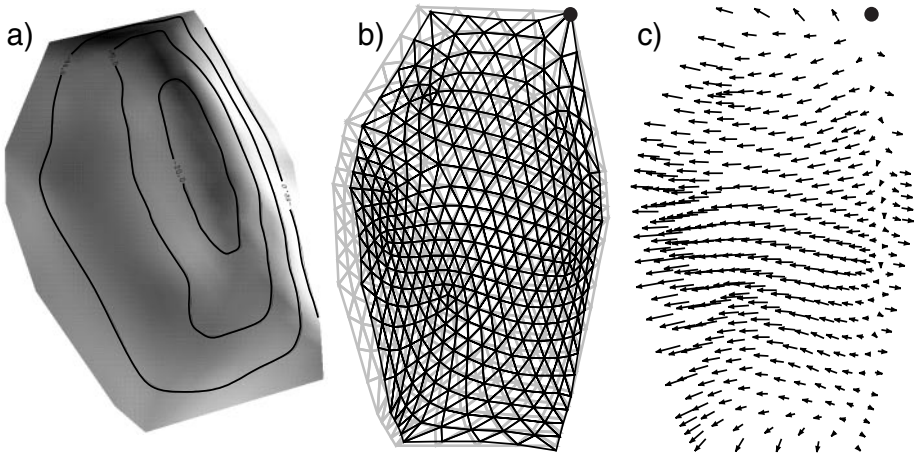

Figure 8—Unfolding of a noncylindrical surface by heterogeneous inclined shear. (a) Perspective view of the folded surface with contour lines (black). (b) Top view of the triangulated surface in the deformed state (shaded) and restored state (black). The shear direction is defined by the dip of the triangles; therefore, the surface has shrunk through the restoration perpendicular to the contour lines. (c) Map view of the folding vectors. The black dot indicates the seed. The folding vectors diverge as a result of the shape of the surface.

the blocks, whereas reverse faults would be overlaps (Figure 9c). We assume the fault displacement is restored when these gaps are closed. Displacements associated with closing the fault gaps are defined relative to a chosen fixed block (shaded block in Figure 9d). To close the gaps, the blocks are packed against the stationary block using rigid-body rotations and translations to achieve a least-square minimization of gaps and overlaps (Figure 9d). The difference between the flattened and restored surfaces gives the field of finite displacement (Figure 9e) due to the faults (the faulting vectors).

Results

If the fully restored state is geometrically consistent with no errors, we assume it to be the undeformed state of the surface; however, restorations will have some error, so we choose restorations with lowest error from the combined unfolding and unfaulting as the best estimations of the undeformed state, as discussed in the following section. The difference between the current (Figure 1a) and the undeformed state (Figure 1c) gives us (1) the 3-D finite displacement field (the sum of the folding vectors and the faulting vectors), (2) the direction of slip on the faults (Figure 1d), and (3) the field of internal strain associated with the unfolding.

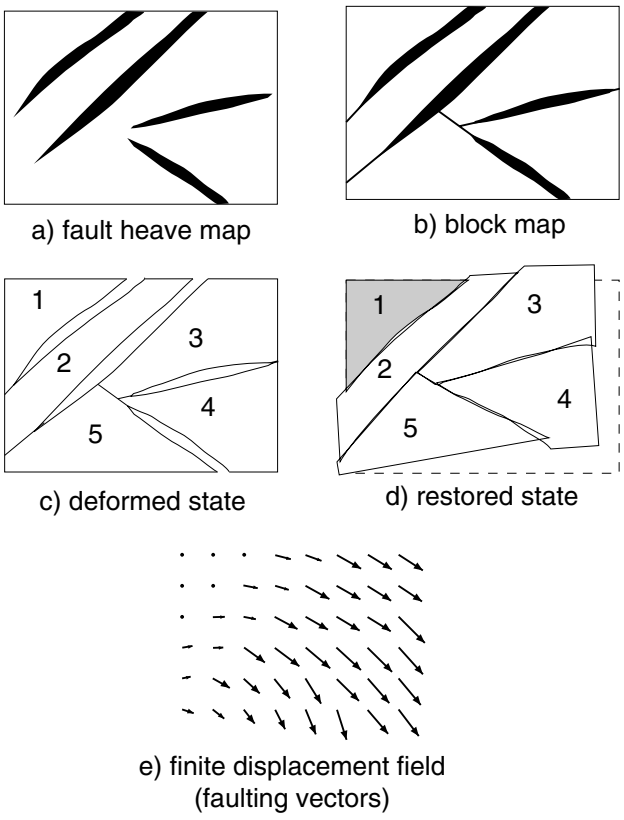

Figure 9—Unfaulting step. From the flattened surface (a), we build a map of fault-bounded blocks (b) separated by gaps representing the normal faults (c). (d) Blocks are sequentially packed against a stationary block (shaded) using rigid-body rotations and translations to minimize gaps and overlaps. (e) The difference between the faulted and restored surface gives the faulting vectors.

APPLICATION TO A GROWTH-FAULT SYSTEM OF THE WESTERN NIGER DELTA

Niger Delta

The Niger Delta has built out over the triple junction of the Gulf of Guinea, the South Atlantic

Ocean, and the Benue depression (Figure 10). The Eocene–Quaternary stratigraphic sequence includes clastic sediments (Benin and Abgada formations) that prograded over marine undercompacted shales (Akata Formation) (Chukwueke et al., 1992) (Figure 11). Systems of growth normal faults deform the clastic sediments. In map view, these arcuate faults trend west-northwest–east-southeast in the northern part of the delta and tend to parallel the delta edges to the south (Figure 10). Each growth fault system involves (1) a seaward-dipping fault (regional fault), (2) an antithetic fault (counterregional fault), and (3) a rollover anticline with secondary faulting (Weber and Daukoru, 1975; Evamy et al., 1978; Doust and Omatsola, 1990).

Our data set is a 3-D seismic survey covering a growth fault system, including the interpretation of six stratigraphic markers and about 60 fault surfaces. The studied area is about 10×10 km in size and is composed of two domains: the footwall and hanging wall of the main fault (F1, Figure 12). The main fault (F1) is associated with synthetic faults (F2 + F3). Fault F2 shows a significant curve and a tip termination toward the south. To the northeast, the relaying synthetic fault (F3) associated with fault F1 is straight. The fault bounding the rollover to the west is synthetic of F1 (Figure 12b). The hanging wall of F1 forms a rollover offset by small synthetic and antithetic faults. The width of fault blocks increases upward. This records the progressive increase in thickness of the sedimentary cover involved in the deformation (Vendeville, 1987; Vendeville and Cobbold, 1987, 1988).

Data and Testing Strategy

We have chosen horizon 2 (Figure 12) to test the method. From the depth-converted horizon 2, we have built a triangulated surface (Figure 13a) following the procedure previously described. The surface consists of two main pieces: the footwall of the fault F1 to the northwest and the hanging wall to the southeast, with numerous gaps corresponding to the secondary faults of the rollover collapse.

The restoration method involves two steps: the unfolding and the unfaulting. We have performed a number of tests to evaluate the sensitivity of the method to (1) the choice of unfolding mechanism, (2) the location of the stationary boundary (pin line and seed) for the unfolding procedure, and (3) the nature of block cutting for the unfaulting steps.

Influence of the Unfolding Mechanism

To evaluate the sensitivity of the method to the unfolding mechanism, we performed 73 restorations with various unfolding mechanisms:

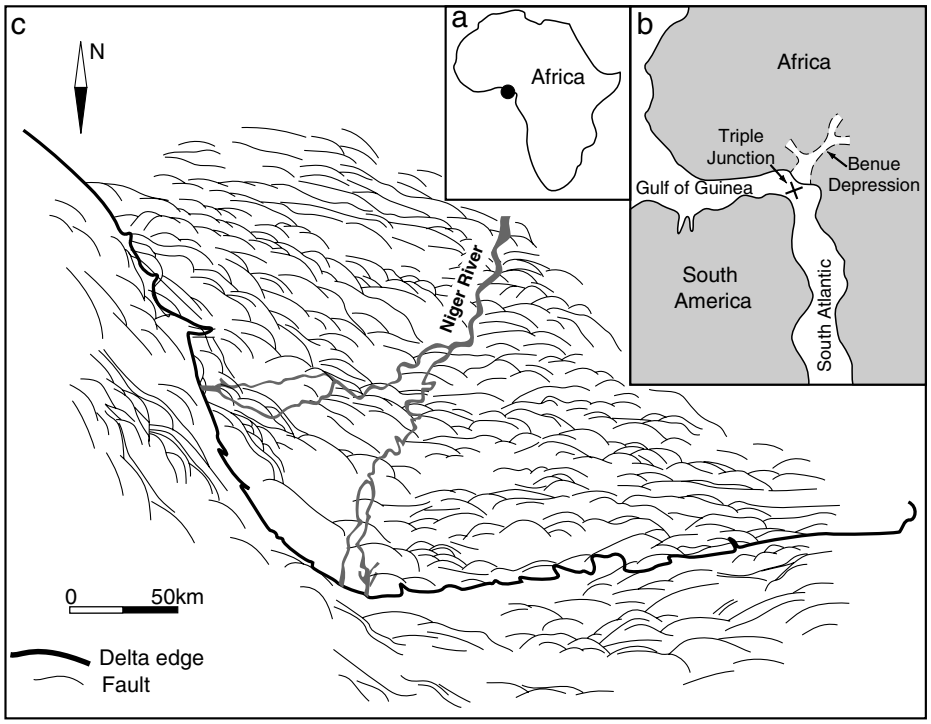

Figure 10—(a) Location of Niger Delta. (b) Early Cretaceous separation of Africa and South America showing the triple junction among the South Atlantic, Gulf of Guinea and Benue depression (modified after Burke et al., 1971). (c) Map of growth faults in the Niger Delta (modified after Weber and Daukoru, 1975).

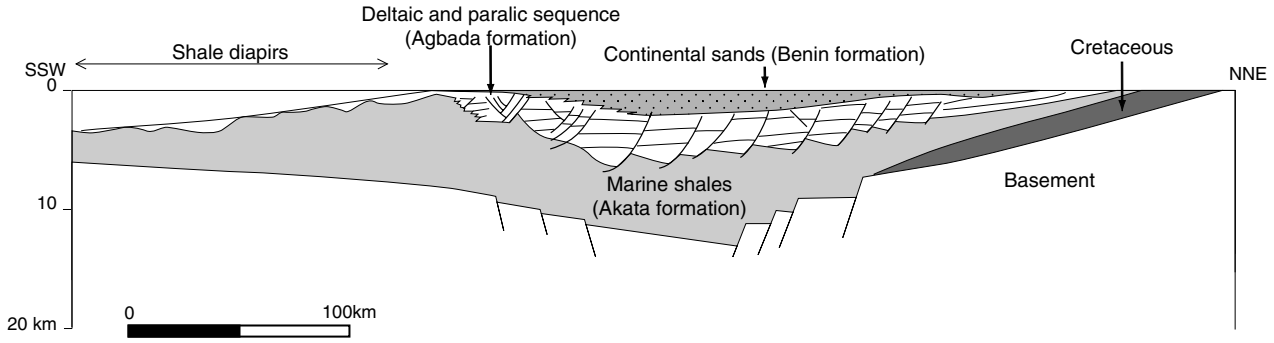

Figure 11—Schematic cross section through the Niger Delta showing the structural position of the three main sedimentary units (modified after Merki, 1972; Evamy et al., 1978; Doust and Omatsola, 1990). Note vertical exaggeration (5:1). See text for explanations.

(1) One restoration by flexural slip (restoration fs)

(2) Thirty-six restorations by homogeneous shear with an azimuth perpendicular to fault F1 and dip angles (antithetic to fault F1) ranging from 55 to 90° (restorations h55–h90)

(3) Thirty-six restorations by heterogeneous shear with dip angle ranging from 55 to 90° (restorations s55 to s90). In this case the azimuth of shear is parallel to the local dip direction of the triangles.

Unfolding

In all cases the pin line is the northeastern side of the footwall with a seed at the northern corner (Figure 13). The depth of the unfolded surface is arbitrarily chosen at the maximum elevation of the folded surface.

As examples, we show the folding vectors for four of the 73 executions: flexural slip (restoration fs, Figures 13b, 14a, 15a), homogeneous inclined shear perpendicular to fault F1 with vectors dipping at 74° from the horizontal (restoration h74, Figures 14b, 15b), and heterogeneous shear with vectors dipping at 55° (restoration s55, Figures 14c, 15c), and 77° (restoration s77, Figures 14d, 15d). Please note that the folding vectors are exaggerated by a factor of three for visibility.

The folding vector maps (Figure 14) show large oblique displacements in the southeastern part of the footwall of the F1 fault, except for the homogeneous case (Figure 14b). The vectors trend in the symmetric direction (i.e., to the south) in the northwestern part of the footwall. This trend suggests the existence of a discontinuity separating a northwestern and a northeastern domain within the footwall. This discontinuity indeed corresponds to a topographic anomaly, a step running north-south through the footwall (labeled "step" in Figure 13) that is probably linked to an uninterpreted fault zone.

For the homogeneous shear example (Figure 14b), the shear vectors are chosen perpendicular to the fault F1, thus the resulting folding vectors mostly trend perpendicularly to the faults. In this example, there is no oblique displacement in the footwall; however, the two displacement domains separated by the discontinuity are clearly visible with displacements larger to the left.

The four folding-vector maps (Figure 14) show larger displacement in the areas of larger initial dip, for example, the area between the F1 fault and the F2-F3 faults. Displacement fields for the two heterogeneous-shear unfoldings are identical except for the displacement magnitudes; the unfolding with shear vectors dipping at 55° shows larger displacements than those dipping at 77° (Figure 14c, d), as expected. The smaller the dip of the antithetic shear vector, the greater the surface dilation.

Maps of shear-strain intensity (the second invariant of the displacement matrix calculated for each triangle) for these four unfoldings are shown as Figure 15. Unfolding by flexural slip gives the smallest shear-strain intensities (Figure 15a), whereas unfolding by heterogeneous shear with vectors dipping at 55° gives the largest (Figure 15c). This finding is consistent with the fact that flexural slip (achieved by rigid rotation of the triangles) preserves the shape of triangles; therefore, the resulting shear strain is related only to the discrepancies of fitting of the triangles. On the contrary, the shear strain computed for the inclined shear also involves the component of shear during the flattening; furthermore, for inclined shear, the areas of larger shear-strain intensities are the areas of larger initial dip. Heterogeneous shear at 77° and homogeneous shear at 74° (Figure 15b, d) give similar strain intensities because the dip of the shear vector is similar.

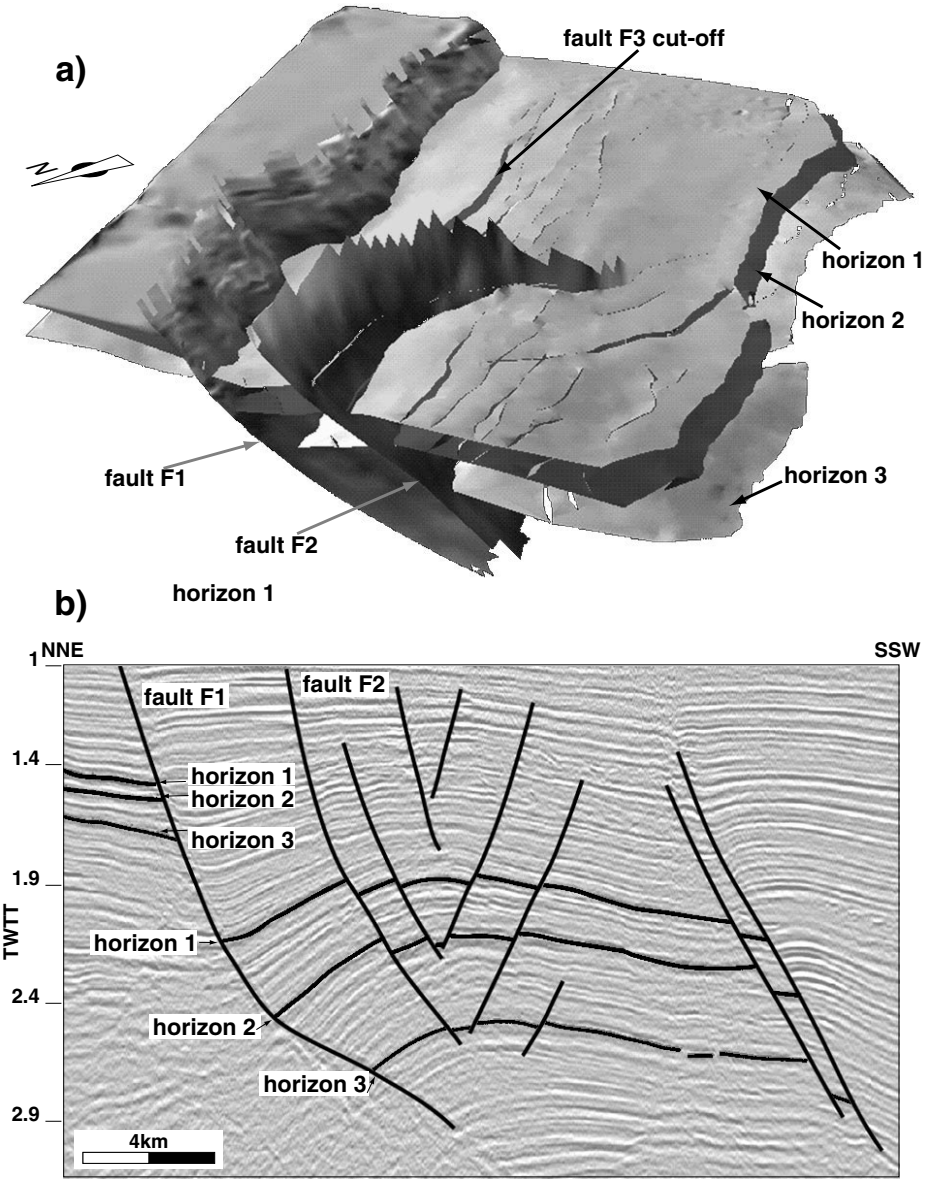

Figure 12—(a) Perspective view of Niger Delta data set showing triangulated surfaces for three horizons, the faults F1 and F2, and the cuts of secondary faults. (b) Interpreted seismic line showing the three horizons and the main faults.

Unfaulting

We cut the unfolded surfaces into mosaics of fault-bounded blocks (Figure 16a). We extrapolated fault traces and segmented elongate blocks using straight block boundaries (see for example the area between fault F1 and F2-F3). We chose the footwall as a stationary boundary (shaded block on Figure 16). The block mosaics are identical for the 73 restorations.

The quality of the fit is evaluated by the area of gap and overlap at the end of the restoration. The initial unrestored map (Figure 16a) shows gaps representing 22% of the surface of the blocks.

The best fit is obtained for the restoration by heterogeneous shear at 77° (restoration s77). Remaining gaps and overlaps represent 0.42% of the surface of the blocks. Figure 16c gives an example of a fit that has been rejected. Restoration s57 (heterogeneous shear with vectors dipping at 57°) was rejected because remaining gaps and overlaps represent 1% of the surface of the blocks. Areas for which the fit has been improved between the two restorations are highlighted.

In addition to restoration s77, other restorations gave an excellent fit (remaining gaps and overlaps represent less than 0.5% of the surface of the blocks): fs (unfolding by flexural slip), h75 (unfolding by homogeneous shear dipping at 75°), and s75 to s80 (unfolding by heterogeneous shear ranging

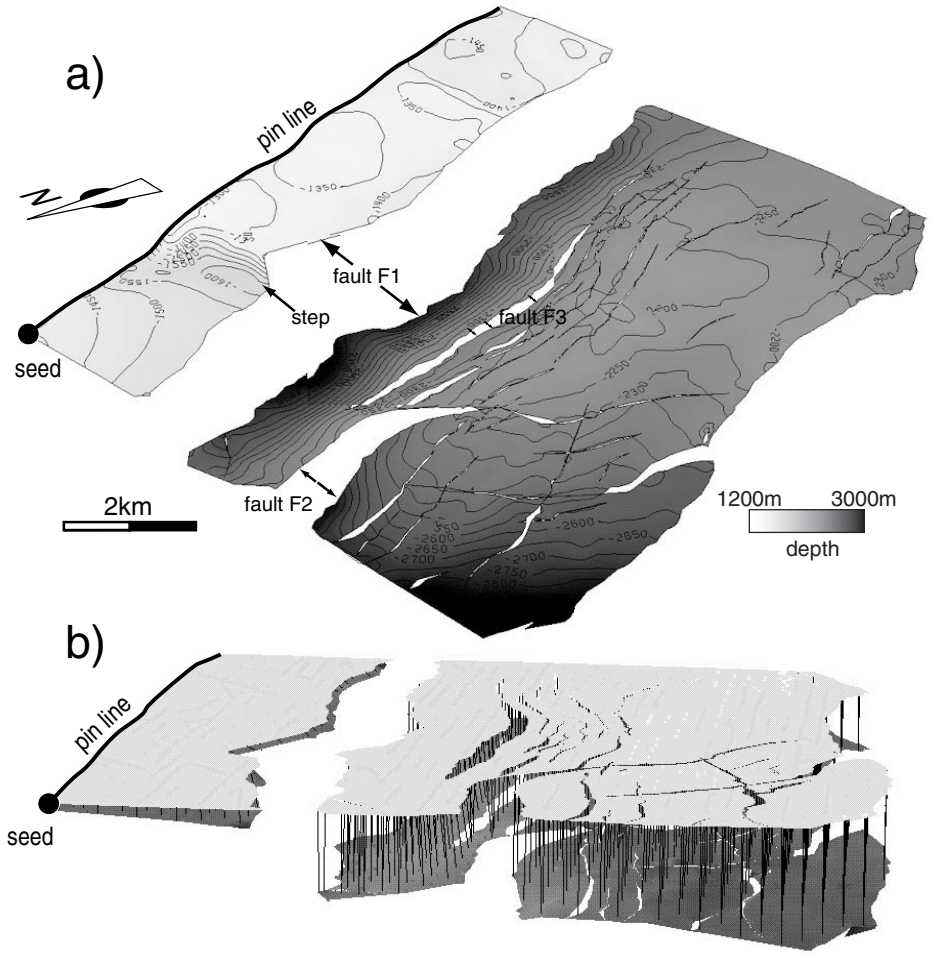

Figure 13—(a) Perspective view of horizon 2 (see Figure 12) with contour lines in black. Pin line and seed used for unfolding are shown. (b) Perspective view of horizon 2 in the folded and unfolded state. Unfolding has been achieved by flexural slip. Folding vectors are shown as black lines.

from 75 to 80° in dip). We will discuss these results in following sections.

3-D Displacement Fields

From the difference between the restored state and the current deformed state, we computed the fields of 3-D finite displacement, which is the sum of the unfolding and the unfaulting (Figures 17, 18). We performed a statistical analysis of the variability of the displacement fields for the 36 executions in homogeneous shear (restoration h55 to h90) and for the 36 executions in heterogeneous shear (restoration s55 to s90). To do so, we compared the vector fields for each vector location. For each location (X, Y), we computed the median vector of the 36 displacement fields. We then computed the deviation of the vectors from this median both in length and direction.

For the homogeneous shear restorations, the median deviation is about 1.5% in length of the vectors and 0.2% (0.4°) in direction. For the heterogeneous shear, the median deviation is about 5.2% in length of the vectors and 0.6% (1.3°) in direction.

For both sets, the variability in angle is lower than in length, indicating that the displacement fields show consistent directions whatever the shear angle and that the variability results mostly from the amount of shear undergone by the surface (directly related to the shear angle). The variability in direction is higher for the restorations by heterogeneous shear than for the restorations by homogeneous shear. This result is consistent with the fact that in the homogeneous case we impose a constant shear direction (but not a displacement direction).

The low variability of the displacement fields with respect to the folding mechanism results from the fact that the displacements related to the folding are small compared to the displacements related to the faults (less than 5% on average). This is to be expected in most of the extensional domains and in many compressional domains. Most of the displacement is accomplished by slip on the mapped faults.

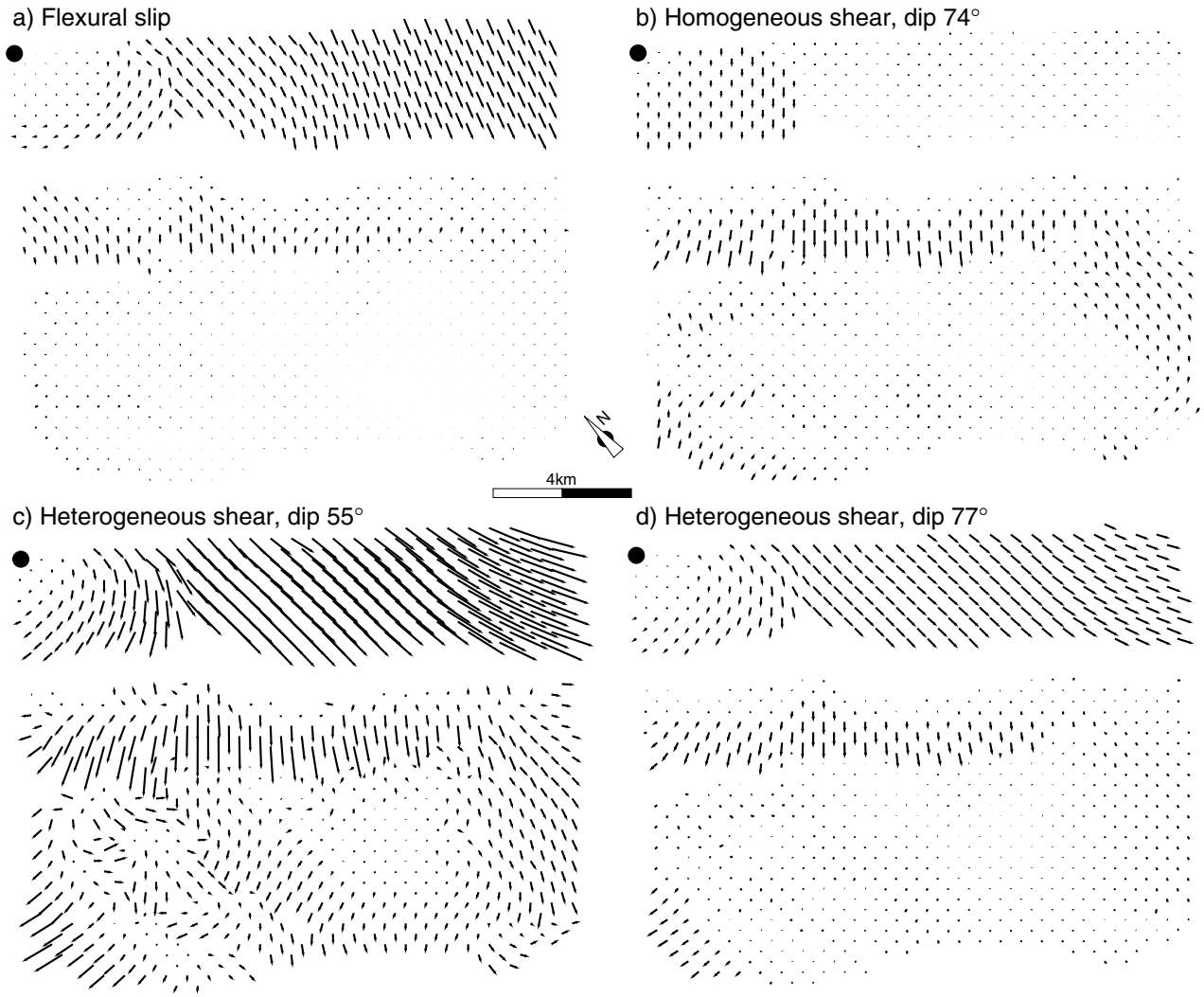

Figure 14—Map view of the folding vectors for four restorations performed using various unfolding mechanisms (the seed is shown as a black dot): (a) flexural slip, (b) homogeneous shear perpendicular to fault F1 with shear vectors dipping at 74° from the horizontal, (c) heterogeneous shear with shear vectors dipping at 55°, and (d) 77°. The lengths of the vectors are multiplied by a factor of three for clarity.

We computed the direction of slip on the faults between the restored and deformed states for the restoration giving the best results (s77, Figure 17c). The main faults show mostly normal slip direction, whereas smaller faults may display some strike-slip component either dextral or sinistral. This component results from the accommodation of rotations of the blocks about vertical axes and, therefore, may be only locally significant. This illustrates how, even though the 3-D displacement field is quite simple (Figure 17b), the distribution of slip on the faults may be much more complicated. This has also been observed on several other examples of complex fault networks (e.g., Rouby et al., 1996a, b; de Urreiztieta et al., 1996; Bourgeois et al., 1997).

Influence of the Stationary Boundary

To evaluate the sensitivity of the method to the stationary boundary during the unfolding, we performed five restorations with different locations of the stationary boundary (seed): the northern corner (Figures 13b, 19a, 20a), the eastern corner (Figures 19b, 20b), the western corner (Figures 19c, 20c), the southern corner (Figures 19d, 20d),

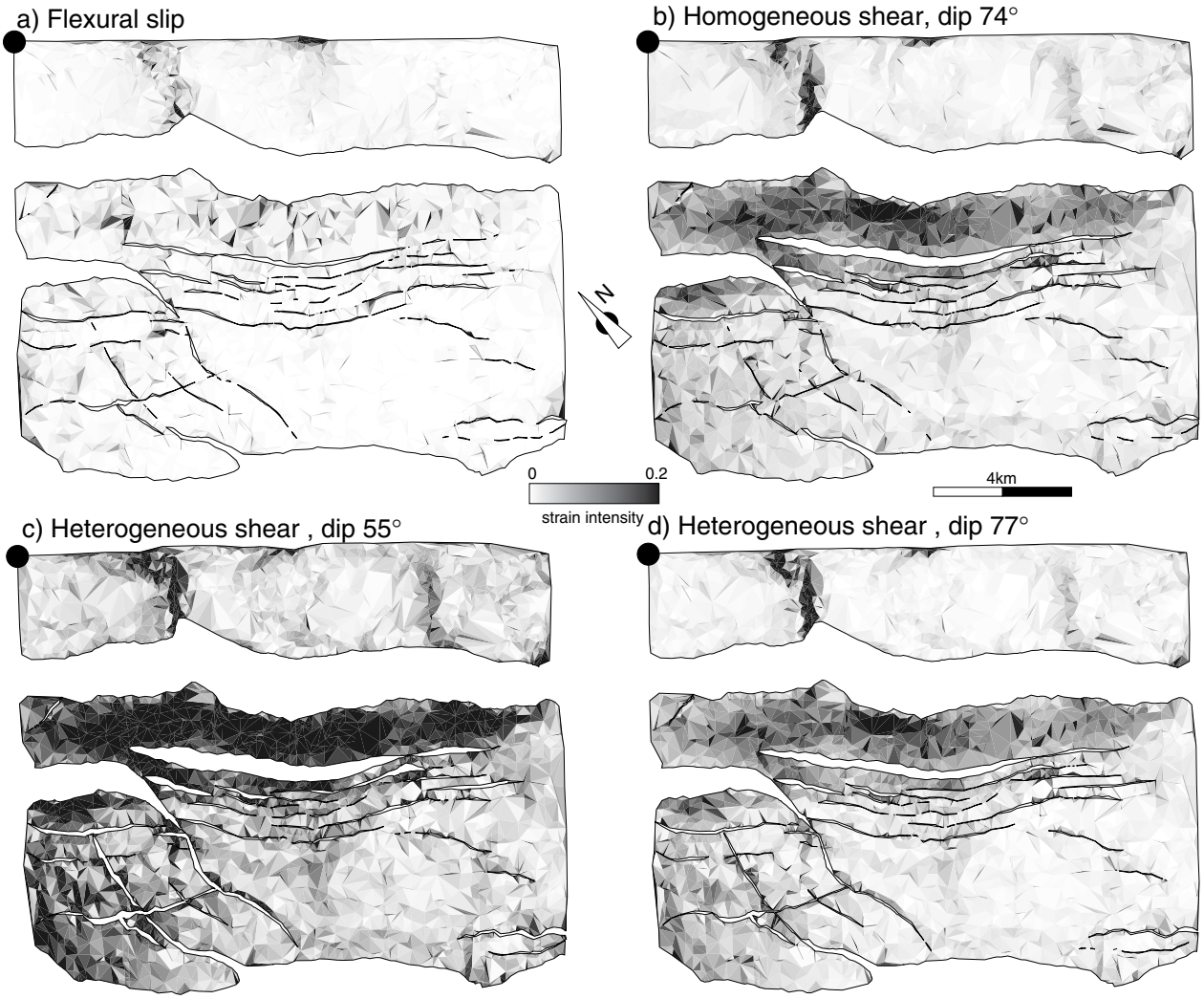

Figure 15—Shear-strain maps for four restorations performed using various unfolding mechanisms (the seed is shown as a black dot): (a) flexural slip, (b) homogeneous shear perpendicular to fault F1 with shear vectors dipping at 74° from the horizontal, (c) heterogeneous shear with shear vectors dipping at 55°, and (d) 77°. Strain values are the second invariant of the displacement matrix calculated within each triangle.

and the center of the hanging wall (Figures 19e, 20e). In each of these cases, the unfolding mechanism is a heterogeneous inclined shear with a dip angle of 65°.

Unfolding

We show the folding vectors for the five restorations (Figure 19). The patterns of the folding vectors look quite different from one execution to the other. This is, however, only an effect of the location of the seed (the displacement amount increase away from the stationary boundary). Indeed, the shear-strain maps, for which this effect is avoided because the shear strain is related only to local displacement gradients, are almost identical (Figure 20). Whatever the location of the seed, the shear-strain maps are consistent with the previous restorations, showing large values along the oblique steep zone within the footwall and between fault F1 and F3.

Unfaulting and 3-D Displacement Fields

From the unfolded surfaces, we built five maps of fault-bounded blocks using the same block mosaic as in the previous set of restorations. From the deformed and unfaulted step, we computed the

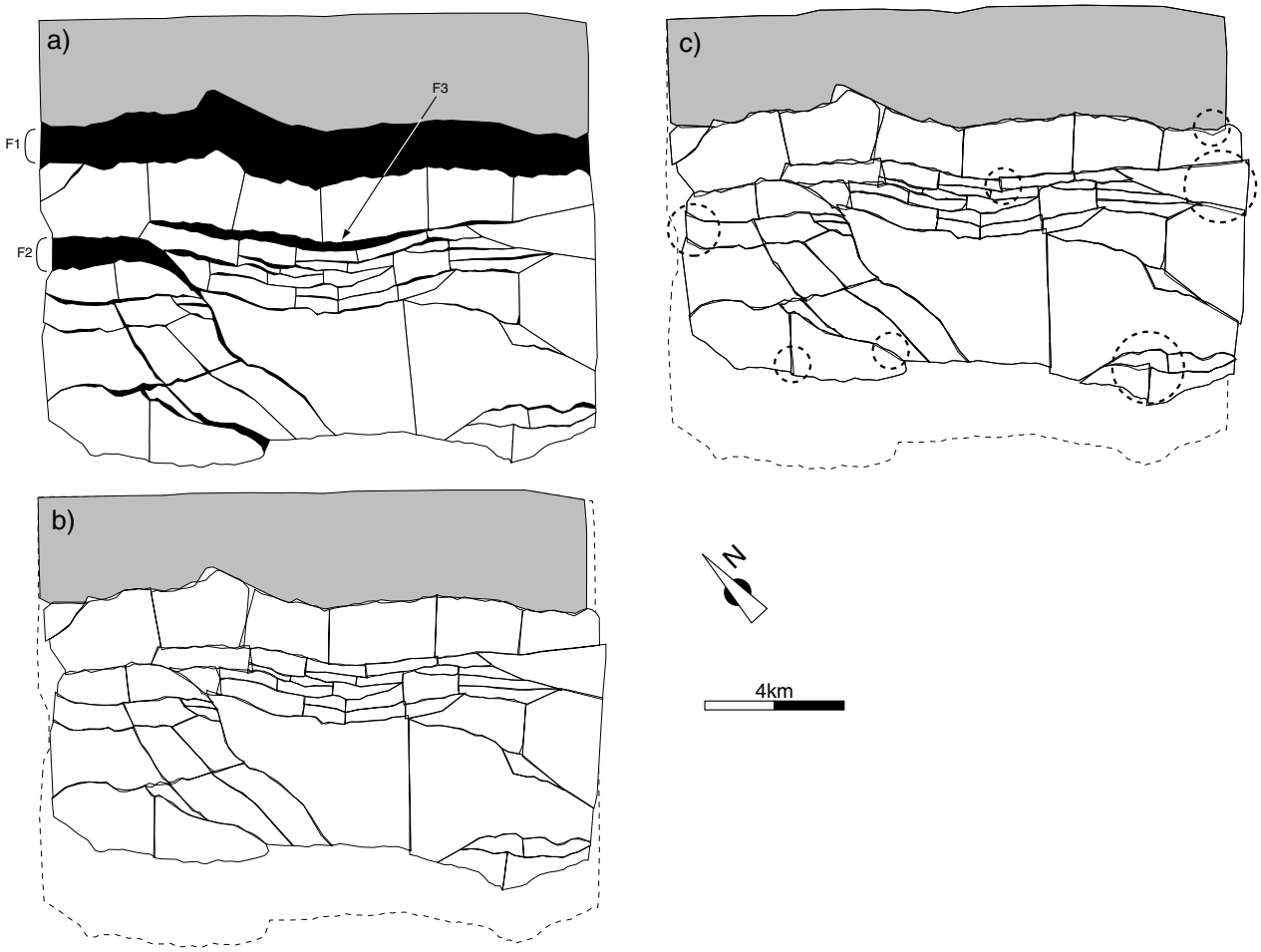

Figure 16—Unfaulting step. (a) Map of fault-bounded blocks. Fault gaps are shown in black, block cuts are shown as straight lines, and blocks are shown as unshaded. The footwall of fault F1 is chosen as the stationary block (shaded). (b) Restored block map giving the best fit (restoration s77). Dashed line indicates the current outline of the map (in the deformed state). (c) Restored block map for another restoration (s57). Thick dashed circles indicate areas where the fit has been improved for restoration s77 shown in (b).

fields of 3-D finite displacements (Figure 21). Because they are the sum of the folding and faulting vectors, they are calculated with respect to the reference point for the whole deformation (the seed).

We analyzed the variability of the 3-D displacement fields. The median deviation is about 1.6% in length and 1.6% (3.6°) in direction. These values are small and lead us to conclude that the location of the seed during the unfolding is not really significant for the computation of the 3-D displacement field.

Influence of the Block Map

To evaluate the sensitivity of the method of cutting the unfolded surface into the block mosaic (extrapolation of the fault traces, introduction of the artificial block boundaries, etc.), we performed four restorations with different block mosaics for the unfaulting step but identical unfolding mechanism (heterogeneous shear at 77°) and seed location (upper left corner).

We show the restored maps for the four different block mosaics (Figure 22). The variability of the 3-D displacement fields is about 0.5% in vector length and 0.2% (0.5°) in direction. These values are small and lead us to conclude that cutting the block mosaic during the unfaulting step is not significant for the computation of the 3-D displacement field.

Although the differences among restorations are small, the block mosaic shown on Figure 22a gives the best fit and corresponds to the block mosaic used in

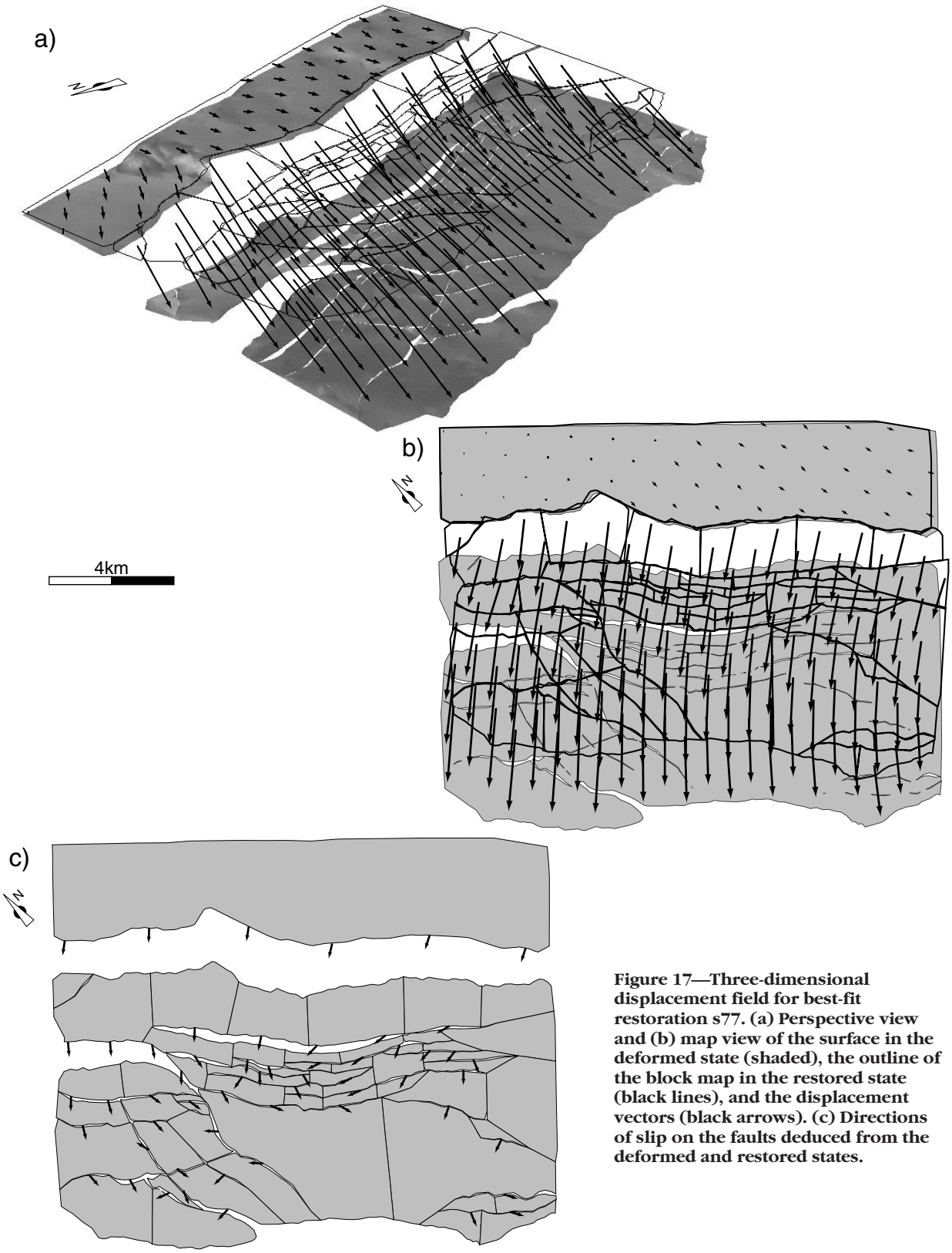

Figure 17—Three-dimensional displacement field for best-fit restoration s77. (a) Perspective view and (b) map view of the surface in the deformed state (shaded), the outline of the block map in the restored state (black lines), and the displacement vectors (black arrows). (c) Directions of slip on the faults deduced from the deformed and restored states.

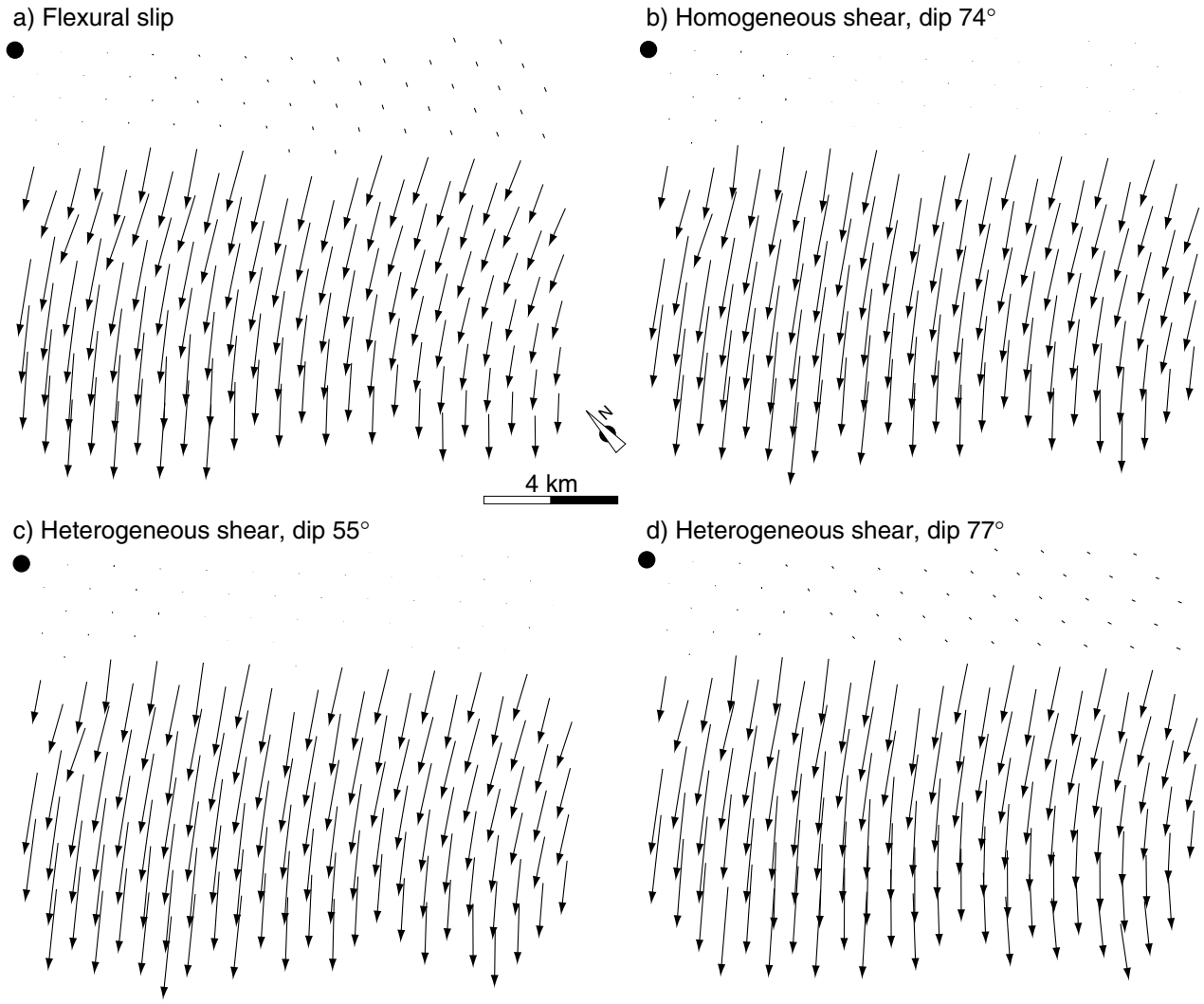

Figure 18—Map view of the 3-D displacement fields for the four restorations shown in Figures 14 and 15.

the previous sets of restoration. The area of remaining gaps and overlaps is 0.42, 0.72, 0.83, and 1% of the block area for the restorations a, b, c, and d, respectively. The small differences in the slip direction from one map to the other are located only on minor faults, suggesting that they have only a local significance.

DISCUSSION

Our new restoration methodology allows the restoration of geological surfaces (1) taking into account the combined displacements related to folding and faulting, (2) including complex fault patterns, and (3) providing a great flexibility in choosing the 3-D folding mechanism (three unfolding options are implemented).

We have based the method of folding and faulting on mechanisms that approximate actual 3-D deformation processes. The unfaulting is by rigid rotation and translation of fault blocks of Rouby et al. (1993a), and the unfolding is by flexural slip of Gratier et al. (1991) that, when combined, represent the 3-D deformation process. To improve the homogeneous inclined shear model (pencil shear, Kerr et al., 1993; Kerr and White, 1996), we included a model of unfolding by heterogeneous inclined shear in which the azimuth of the unfolding vector is parallel to the local dip of the surface. We argue that there is no reason why the folding direction above

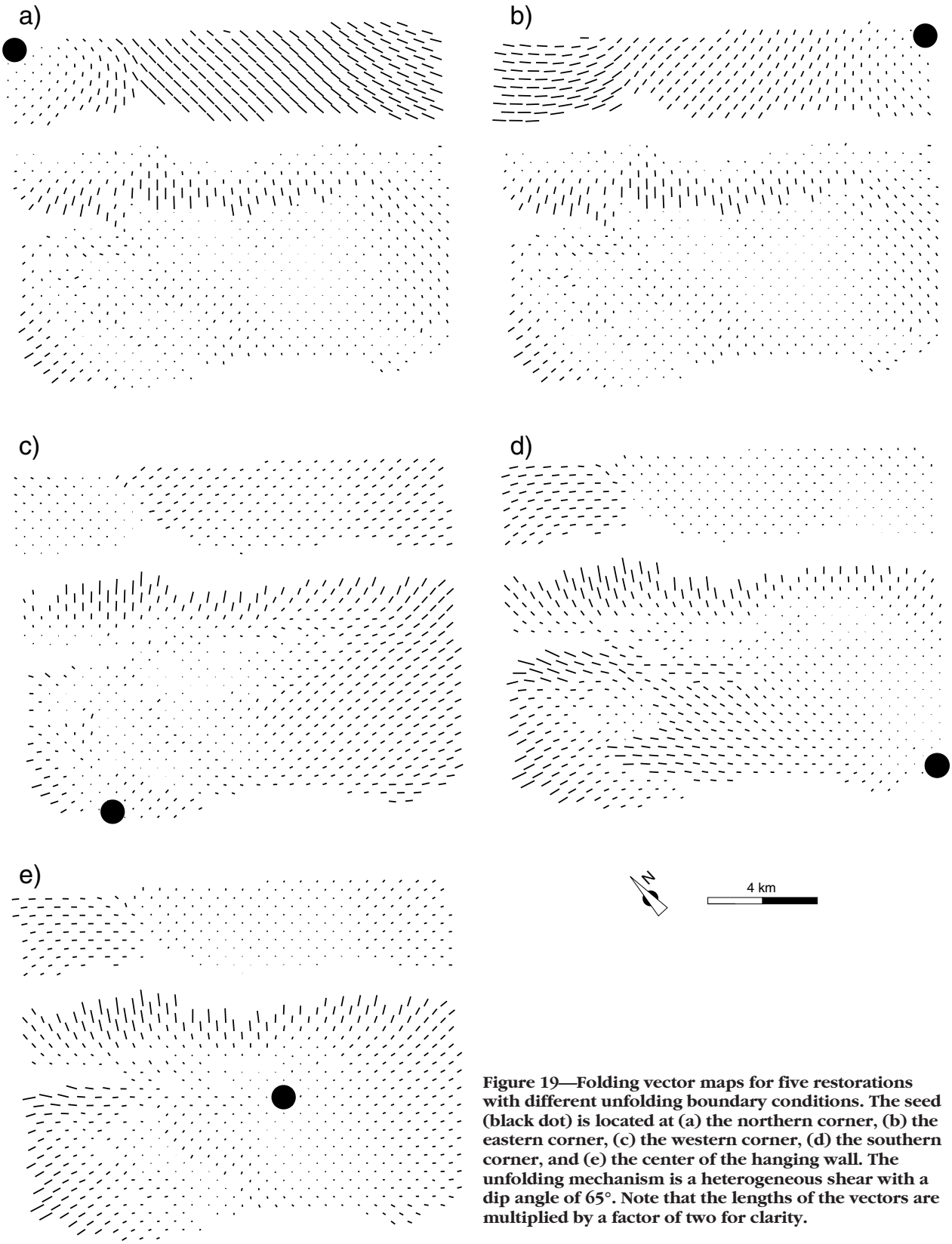

Figure 19—Folding vector maps for five restorations with different unfolding boundary conditions. The seed (black dot) is located at (a) the northern corner, (b) the eastern corner, (c) the western corner, (d) the southern corner, and (e) the center of the hanging wall. The unfolding mechanism is a heterogeneous shear with a dip angle of 65°. Note that the lengths of the vectors are multiplied by a factor of two for clarity.

Figure 20—Shear-strain maps for the five restorations with different seed locations (black dots) of Figure 19. Note that the strain patterns are insensitive to the seed location.

an irregular fault surface or within a complex 3-D fault network should, in general, be homogeneous, and thus suggest that heterogeneous shear is necessary to properly restore complexly faulted systems.

Heterogeneous Inclined Shear

The underlying assumption of heterogeneous inclined shear is that the displacement directions follow the gradients of topography of the deformed surface. This model needs further testing and other mechanisms are geologically conceivable; however, we believe that it is the most consistent way to make use of the main geological information to which we have access in performing the restoration, that is, the current (deformed) shape of the geological horizons. It can be argued that other information should be used, for example, the shape of the fault surfaces; however, faults are generally not well defined, especially at depth. In addition, there are strong indications that growth faults rotate through time (e.g., Vendeville and Cobbold, 1988; Rouby and Cobbold, 1996), suggesting that these faults cannot be used as a simple boundary condition.

A shortcoming of this heterogeneous inclined shear model is as follows. Although the azimuth of the shear vectors is locally defined (and therefore is not homogeneous), the dip of the shear vectors, on the contrary, is still (1) defined by the user and, as a consequence, (2) remains constant throughout the restored area.

(1) The choice of the dip angle of the shear vectors by the user can seem quite difficult and subjective. The geologist can be helped by the dip of the axial surfaces associated with the folds, following Xiao and Suppe (1992); however, the axial surfaces are not always visible on the data, especially when faults are curved and have no abrupt bend. To avoid this "arbitrary" choice, we have designed the software so that the user can perform multiple restorations with various folding mechanisms and shear angles. The user can determine a more appropriate unfolding mechanism, assuming that the restoration giving the best geometrical fit is the one corresponding to the most geologically consistent folding mechanism.

In this paper, the best fits are obtained for unfolding by heterogeneous inclined shear antithetic to the main fault with shear vector dips ranging from 75 to 80° (best fit for 77°). These shear angles are compatible with 2-D forward modeling of cross sections from the same growth fault system using the method of Xiao and Suppe (1992), which gave best results with an antithetic shear angle between 70 and 75°. The consistency of the results of the heterogeneous shear between 75 and 80° makes it the most appropriate choice. In contrast, restorations using a homogeneous shear of between 70 and 80° gave fits exceeding 0.5% of gaps and overlaps. The restoration by flexural slip also gave a good fit and is again related to the fact that folding vectors are small with respect to faulting vectors; however, flexural slip has given very poor results for cross section modeling.

These results show that the multiple restoration optimization procedure can help the user determine the appropriate unfolding mechanism, but in cases of small folding displacements, the discrimination between the best fits might not be easy, and thus the user needs to apply the restoration to several horizons within the growth structure and choose the unfolding mechanism that is the most appropriate, on average, to the whole structure.

(2) When achieving the unfolding by heterogeneous shear, the dip of the shear vectors remains constant throughout the restored area. To perform a fully 3-D unfolding by inclined shear, it should be possible to define locally the dip of the shear vector, just as the azimuth is defined by the local dip azimuth of the surface. There is no reason to assume a constant shear angle above a nonplanar fault surface or within a complex fault pattern; however, at present, we lack the criteria that would allow us to do so. More observations of geological data sets need to be made. It will be an important line of research to design a restoration method that would provide the dip of the shear vectors as a result of the reconstruction (similar to the direction of slip on the fault being the result of our block packing), rather than input data as is presently the case.

3-D Volume Restoration

Before developing full 3-D volume restoration, significant questions concerning the deformation processes in three dimensions need to be answered. These questions include asking how the horizons are linked in three dimensions during the deformation. In other words, when one is restoring the horizons by backstripping, how is the displacement deduced from the top horizon to the underlying horizons?

This problem is already faced when restoring in cross section. In this case, the displacement measured on the top horizon is simply propagated vertically (or along the shear vectors for the inclined shear) to the underlying horizons. This assumption

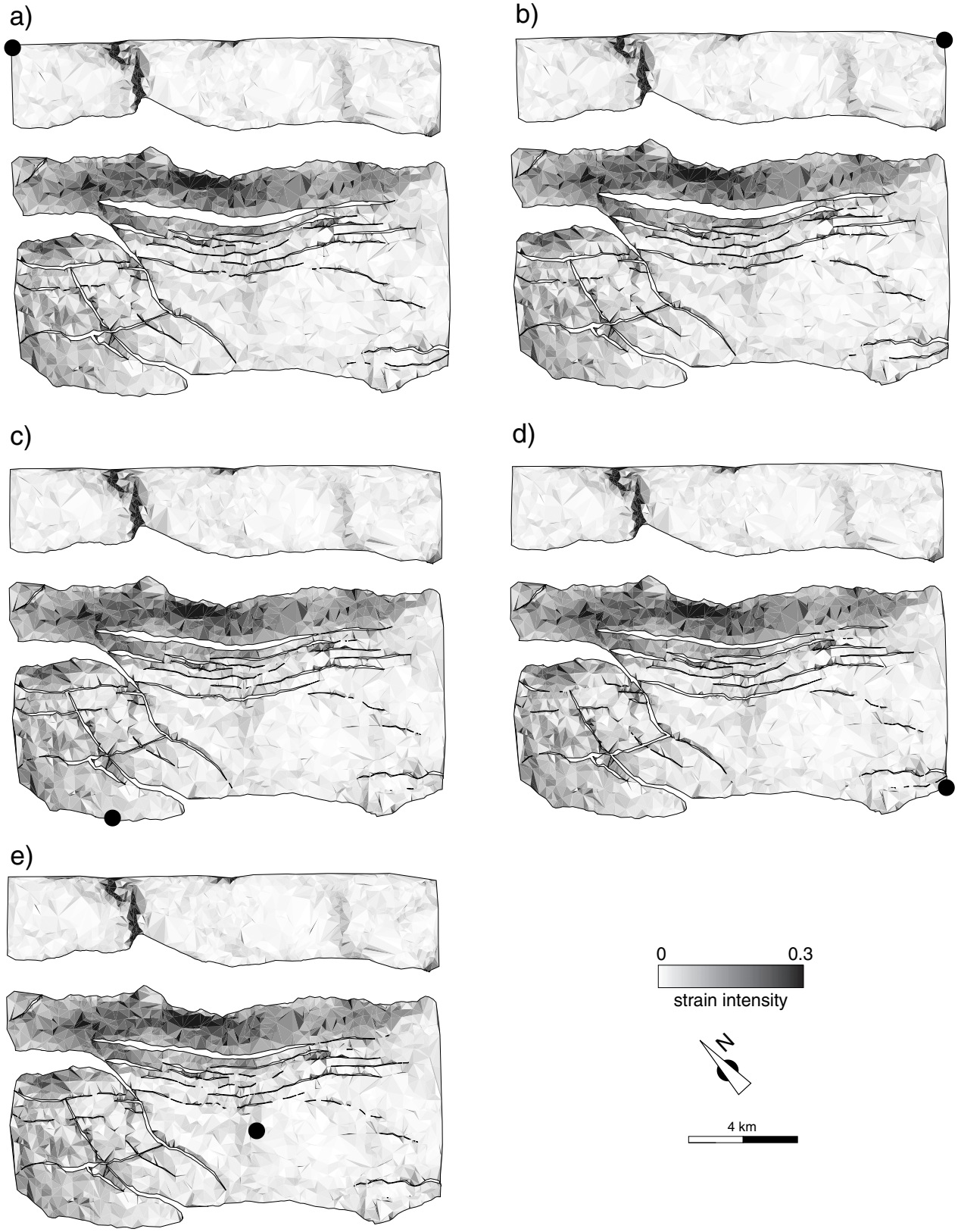

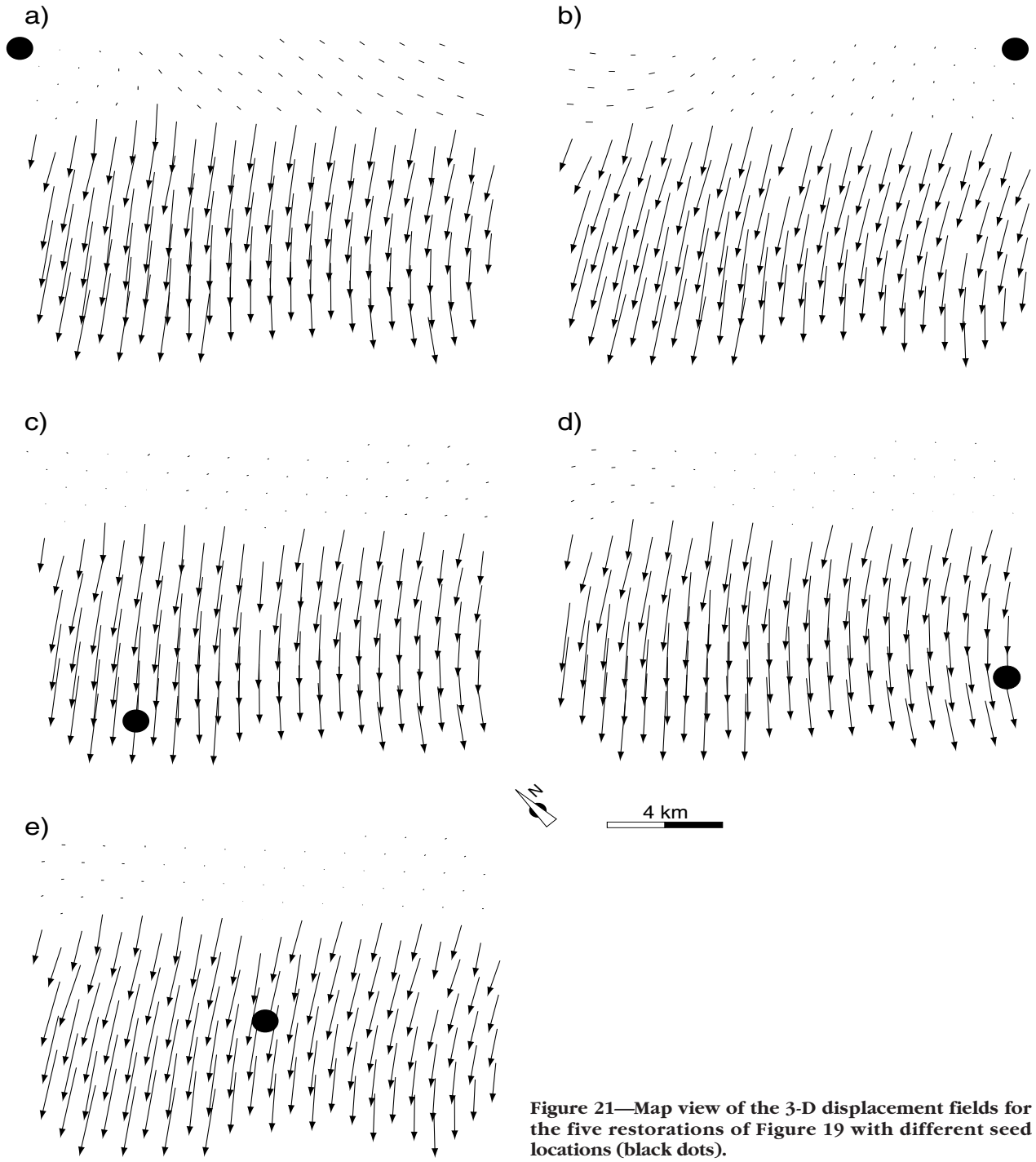

Figure 21—Map view of the 3-D displacement fields for the five restorations of Figure 19 with different seed locations (black dots).

may be satisfactory in many cases in cross section, but it cannot be applied directly in three dimensions because the displacement fields are truly 3-D and cannot be simplified to a vertical propagation. This would also ignore the presence of faults that are by definition discontinuities across which the displacement fields are different.

We think that our new method can help us understand the deformation processes in three dimensions and address the issue of how to propagate

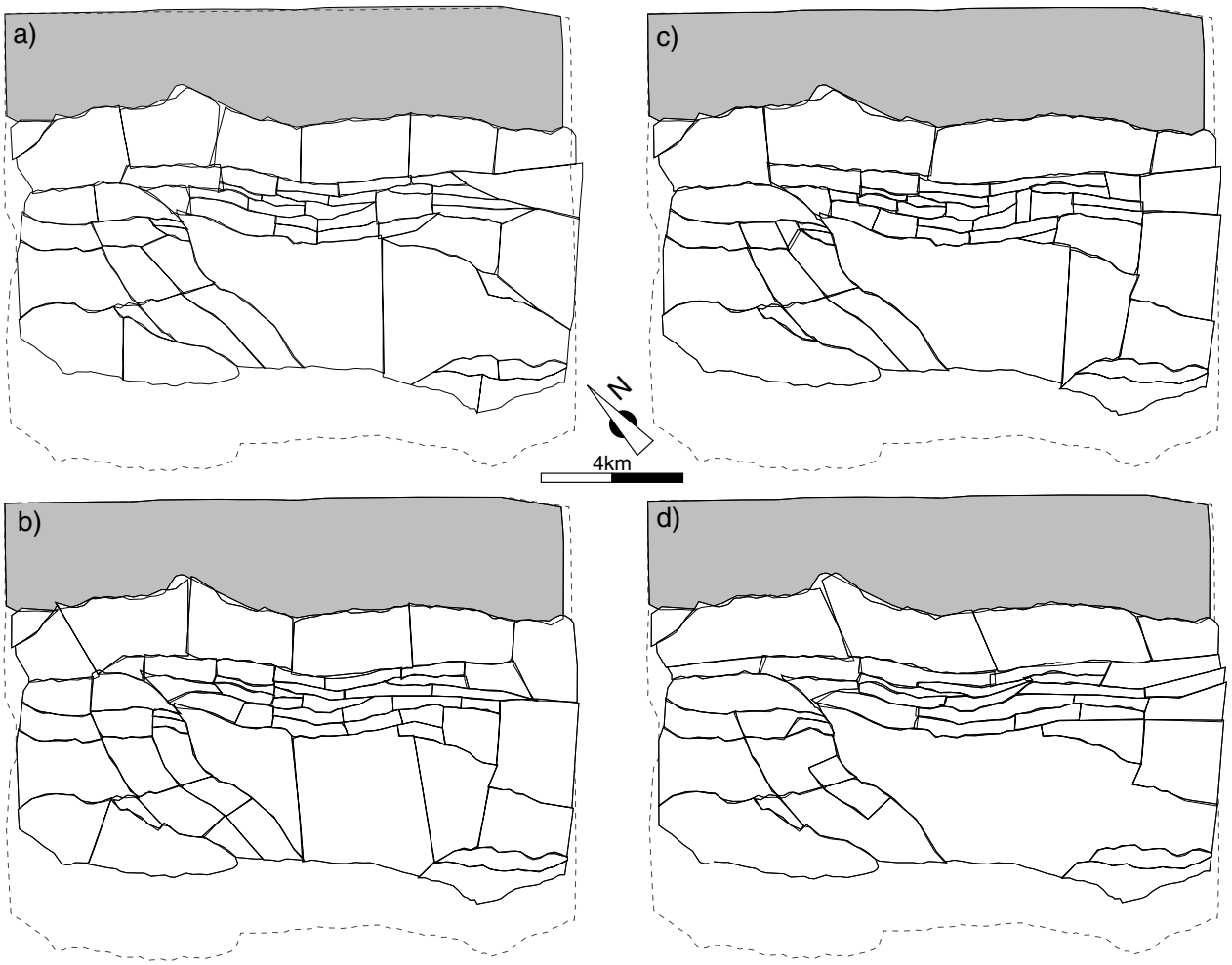

Figure 22—Map view of four different block mosaics in the restored state, showing that the block cuts have little overall effect but can be locally important (see text for explanation).

displacement vectors downward in the geological volume. The next step would be to apply the method to several horizons within the same basin and then compute incremental displacement fields for time intervals between the deposition of the horizons. In doing so on several examples, we can (1) determine the geometrical relationships between the horizons in terms of deformation and displacements and (2) measure the rates of deformation and their variations through time. In doing so, one could gain significant insights into the behavior of a deforming geological volume. This approach has been used already with the restoration method in map view on a growth fault structure of the Niger Delta (Rouby and Cobbold, 1996). It has been shown that the computation of incremental displacement fields describes the history of the structure. In this case, the progressive curvature of a growth normal fault, which initiated as a straight fault and progressively rotated toward horizontal, has been recorded.

CONCLUSIONS

We have presented a method of 3-D restoration of complexly faulted and folded surfaces that is based on features of earlier unfolding and unfaulting techniques. The resulting method is sufficiently robust and streamlined. The entire process is optimized such that the best-fitting unfolding mechanism can be evaluated. Three main types of results can be computed from the restoration.

(1) The 3-D displacement field, sum of folding and faulting vectors, gives us valuable information about kinematics of deformation. The tests of the

new restoration method have shown that neither the cutting of the block mosaic introduced for the unfaulting step nor the location of the stationary boundary for the unfolding step seem to have a significant influence on the 3-D displacement field. This result is due, in part, to the case studied here, where the folding displacements are small compared to the fault displacements. This should be expected in many extensional environments.

(2) The direction of slip on the faults, which is usually an assumption of most restoration methodology, is determined by this method and can be used to analyze the behavior of fault blocks within the general frame of the 3-D displacement field. We show that even with a simple 3-D displacement field, the distribution of slip on the faults may be complicated. High variations of slip directions on small faults can be of only local significance.

(3) Surface strains are computed from remaining discrepancies after triangular element fitting. Strain maps can be interpreted as indicating subseismic deformation processes. Restoration allows high-strain areas to be predicted and, therefore, might be a significant help for reservoir analysis and modeling.

REFERENCES CITED

Audibert, M., 1991, Déformation discontinue et rotation de blocs: méthodes numériques de restauration: Application à la Galilée: Mémoires et Documents du Centres Armoricain d'Etudes Structurales des Socles, v. 40, 239 p.

Bourgeois, O., P. R. Cobbold, D. Rouby, and J. C. Thomas, 1997, Least square restoration in plan view of tertiary thrust sheets in the Tadzhik depression, central Asia: Journal of Geophysical Research, v. 102, p. 27,553–27,573.

Burke, K. C., T. F. Dessauvagie, and A. J. Whiteman, 1971, The opening of the Gulf of Guinea and the geological history of the Benue depression and Niger delta: Nature, v. 233, p. 51–55.

Chukwueke, C., G. Thomas, and J. Delfaud, 1992, Processus sédimentaires, eustatisme, subsidence et flux thermique dans la partie distale du Delta du Niger: Bulletin des Centres de Recherches et Exploration-Production de Elf Aquitaine, v. 16, p. 137–186.

Cobbold, P. R., and M. N. Percevault, 1983, Spatial integration of strain using finite elements: Journal of Structural Geology, v. 5, p. 299–305.

Dahlstrom, C. D. A., 1969, Balanced cross section: Canadian Journal of Earth Science, v. 6, p. 743–757.

de Urreiztieta, M., 1996, Tectonique néogène et bassins transpressifs en bordure méridional de l'Altiplano-Puna (27°S), Nord-Ouest argentin: Mémoires de Geosciences, v. 72, 311 p.

de Urreiztieta, M., O. Bourgeois, D. Gapais, P. R. Cobbold, C. Lecorre, E. Rossello, and D. Rouby, 1996, Restoration in map view of the Pampean Ranges province, southern edge of the Puna Plateau, Argentina: Third ISAG (International Symposium on Andean Geodynamics), St. Malo, France, p. 517.

Dokka, R. K., and C. J. Travis, 1990, Late Cenozoic strike-slip faulting in the Mojave Desert, California: Tectonics, v. 9, p. 311–340.

Doust, H., and E. Omatsola, 1990, Niger Delta, *in* J. D. Edwards and P. A. Santogrossi, eds., Divergent/passive margins: AAPG Memoir 48, p. 201–238.

Evamy, B. D., J. Haremboure, P. Kamerling, W. A. Knaap, F. A. Molloy, and P. H. Rowlands, 1978, Hydrocarbon habitat of Tertiary Niger Delta: AAPG Bulletin, v. 62, p. 1–39.

Gibbs, A. D., 1983, Balanced cross-section construction from seismic sections in areas of extensional tectonics: Journal of Structural Geology, v. 5, p. 153–160.

Gratier, J. P., and B. Guillier, 1993, Compatibility constraints on folded and faulted strata and calculation of total displacement using computational restoration (UNFOLD program): Journal of Structural Geology, v. 15, p. 391–402.

Gratier, J. P., B. Guillier, A. Delorme, and F. Odonne, 1991, Restoration and balanced cross section of a folded and faulted surface by computer program: principle and application: Journal of Structural Geology, v. 13, p. 111–115.

Guillier, B., 1991, Dépliage automatique de strates plissées et faillées: application à l'équilibrage des structures naturelles: Ph.D. thesis, University of Grenoble, Grenoble, France, 160 p.

Hossack, J. R., 1979, The use of balanced cross section in the calculation of orogenic contraction: a review: Journal of the Geological Society London, v. 136, p. 705–711.

Kerr, H., and N. White, 1996, Application of an inverse method for calculating three dimensional fault geometries and slip vectors, Nun River field, Nigeria: AAPG Bulletin, v. 80, p. 432–444.

Kerr, H., N. White, and J. P. Brun, 1993, An automatic method for determining 3-Dimensional normal fault geometry: Journal of Geophysical Research, v. 98, p. 17,837–17,857.

Mallet, J. L., 1992, Discrete smooth interpolation in geometric modeling: Computer Aided Design, v. 24, p. 178–191.

Merki, P., 1972, Structural geology of the Cenozoic Niger delta, *in* T. F. Dessauvagie and A. J. Whiteman, eds., African geology: Nigeria, University of Ibadan, p. 635–646.

Richard, S. M., 1993, Palinspastic reconstruction of southeastern California and southwestern Arizona for the middle Eocene: Tectonics, v. 12, p. 830–854.

Rouby, D., and P. R. Cobbold, 1996, Kinematic analysis of a growth fault system in the Niger Delta from restoration in map-view: Marine and Petroleum Geology, v. 13, p. 565–580.

Rouby, D., P. R. Cobbold, P. Szatmari, S. Demercian, D. Coelho, and J. A. Rici, 1993a, Least-squares palinspastic restoration of regions of normal faulting: application to the Campos basin (Brazil): Tectonophysics, v. 221, p. 439–452.

Rouby, D., P. R. Cobbold, P. Szatmari, S. Demercian, D. Coelho, and J. A. Rici, 1993b, Restoration in plan view of faulted Upper Cretaceous and Oligocene horizons and its bearing on the history of salt tectonics in the Campos Basin (Brazil): Tectonophysics, v. 228, p. 435–445.

Rouby, D., H. Fossen, and P. R. Cobbold, 1996a, Extension, displacement and block rotations in the lager Gullfaks area, northern North Sea, as determined from plan view restoration: AAPG Bulletin, v. 80, p. 875–890.

Rouby, D., T. Souriot, J. P. Brun, and P. R. Cobbold, 1996b, Displacements, strains and rotations within the Afar depression (Djibouti) from restoration in map-view: Tectonics, v. 15, p. 952–965.

Samson, P., 1996, Equilibrage de structures géologiques 3D dans le cadre du projet GOCAD: Thèse d'ingénieur, Institut National Polytechnique de Lorraine, Lorraine, France, 222 p.

Schultz-Ela, D. D., 1992, Restoration of cross sections to constrain deformation processes of extensional terranes: Marine and Petroleum Geology, v. 9, p. 372–388.

Schwerdtner, W. M., 1977, Geometric interpretation of regional strain analyses: Tectonophysics, v. 39, p. 515–531.

Vendeville, B., 1987, Champs de failles et tectonique en extension: modélisation experimentale: Mémoires et Documents du Centres Armoricain d'Etudes Structurales des Socles, v. 15, 395 p.

Vendeville, B., and P. R. Cobbold, 1987, Glissements gravitaires synsédimentaires et failles normales listriques: modèles expérimentaux: Comptes Rendus de l'Académe des Sciences de Paris, v. 305, p. 1313–1319.

Vendeville, B., and P. R. Cobbold, 1988, How normal faulting and sedimentation interact to produce listric fault profiles and stratigraphic wedges: Journal of Structural Geology, v. 10, p. 649–659.

Verral, P., 1981, Structural interpretation with application to North Sea problem: London, Joint Association of Petroleum Courses (JAPEC), Course Notes no. 3, unpaginated.
Weber, K. J., and E. Daukoru, 1975, Petroleum geology of the Niger Delta: Proceedings of the Ninth World Petroleum Congress, Tokyo, v. 2, p. 209–221.
White, N., J. A. Jackson, and D. P. McKenzie, 1986, The relationship between the geometry of normal fault and that of the sedimentary layers in their hanging walls: Journal of Structural Geology, v. 8, p. 897–909.
Williams, G. D., S. J. Kane, T. S. Buddin, and A. J. Richards, 1997, Restoration and balance of complex folded and faulted rock volumes: flexural flattening, jigsaw fitting and decompaction in 3D: Tectonophysics, v. 273, p. 203–218.
Xiao, H. B., and J. Suppe, 1992, Origin of rollover: AAPG Bulletin, v. 76, p. 509–529.

ABOUT THE AUTHORS

Delphine Rouby

Delphine Rouby received a Ph.D. in structural geology from the University of Rennes (France) in 1994, where she is presently a research scientist for the CNRS. Her field of research is the intercations between tectonics and sedimentation and three-dimensional restoration.

Hongbin Xiao

Hongbin Xiao received his B.S. degree from Zhejiang University (1982), an M.S. degree from the University of Massachusetts at Amherst (1985), and a Ph.D. from Princeton University (1990). After working as a consulting structural geologist in Chevron Petroleum Technology Company for six years, he spent the next three years exploring for hydrocarbon in PNG fold-and-thrust belt for Chevron Nuigini. He returned to Chevron Petroleum Technology in 1999, where he is working on topics of three-dimensional structural geometry with emphasis on salt tectonics.

John Suppe

John Suppe is Blair Professor of Geosciences at Princeton University. He directs the Princeton 3-D Structures Project, which explores the fundamental processes of deformation that are important within petroleum basins.